

MULTISCALE CHARACTERIZATION OF AN EXTENSIVE STROMATOLITE FIELD: A NEW CORRELATION HORIZON FOR THE CRATO MEMBER, ARARIPE BASIN, BRAZIL

LUÍS FERNANDO SILVEIRA,^{1,2} LEONARDO BORGHI,² FABIA EMANUELA RAFALOSKI BOBCO,² BRUNO CÉSAR ARAÚJO,² MATEUS KROTH,^{1,2} GUILHERME DUARTE,² LAÍS DE OLIVEIRA FERREIRA,² AND JOALICE DE OLIVEIRA MENDONÇA³

¹Universidade Federal do Rio de Janeiro, CCMN/IGEO, Programa de Pós-Graduação em Geologia, Avenida Athos da Silveira Ramos 274, Bloco J1, Cidade Universitária, 21941-916, Rio de Janeiro, RJ, Brazil

²Universidade Federal do Rio de Janeiro, CCMN/IGEO, Departamento Geologia, Laboratório de Geologia Sedimentar, Avenida Athos da Silveira Ramos, 274, Sala J1-11, 21941-916, Rio de Janeiro, RJ, Brazil

³Universidade Federal do Rio de Janeiro, CCMN/IGEO, Departamento Geologia, Laboratório de Palinofácies e Fácies Orgânica, Avenida Athos da Silveira Ramos 274, Sala J1-20, 21941-916, Rio de Janeiro, RJ, Brazil
email: luis@geologia.ufrj.br

ABSTRACT: There is wide recognition of lacustrine sediments as excellent archives of a basin's depositional history due to their high sensitivity to environmental changes. Among them, microbial limestones are one of the most valuable tools for paleoenvironmental reconstruction, because the biological agents responsible for their genesis tend to respond to short-lived variations of the depositional setting creating specific precipitation patterns. We here document and investigate the sedimentary features of a specific sedimentary layer, remarkable by the extraordinary lateral continuity of its textural attributes over kilometer distances. This marker horizon occurs among the first carbonate layers of the Crato Member (Aptian, Araripe Basin, NE Brazil), commonly assigned a paleolacustrine system. We build on a multiscale comparative analysis (mesoscale, microscale, and chemical) to outline the main processes and paleoenvironmental settings that prompted this interval's widespread and laterally nearly uniform deposition. A lamination pattern identified in different well cores was scrutinized and compared, and shows striking lateral continuity attesting to autochthonous biologically induced mineralization as the primary mechanism of the formation of the microbialites. Compositional and stable-isotope results also show similar trends throughout the well cores, where minor differences represent the influence of local processes.

The studied interval encompasses the relatively swift transition of organic shales rich in ostracod valves to planar stromatolites, where both developed in the anoxic benthonic zone of a freshwater lake. The precipitation of the overlying thinly laminated limestones is related to a change in the carbonate genetic mechanism as a response to a more stable lacustrine stratification. The widespread formation of microbialites preserving an almost identical textural pattern must be related to a regional event, constituting a rare example of a preserved ancient biostrome. Moreover, the investigation of this sedimentary layer can further contribute to determining the roles of different biotic and abiotic processes in microbialite precipitation over large areas.

INTRODUCTION

Lacustrine sediments can be high-resolution archives of the environmental history of a basin, including its physical, biological, and chemical changes (Kelts and Talbot 1990). These deposits commonly preserve original sedimentary textures and isotopic records, often allowing precise reconstructions of the environmental settings (e.g., Kelts and Talbot 1990; Lamb et al. 2007; Doebbert et al. 2014; Baddouh et al. 2017; Letterón et al. 2017). Even though many lakes precipitate carbonates at some point in their depositional history, distinct carbonate facies can express subtle changes in dynamic environmental settings. Organomineralization (Trichet and Défarge 1995) has also been cited as having a significant role in the precipitation of carbonates in lacustrine settings, especially in the nearshore zones, by the interactions of microbial metabolism and

environmental conditions, eventually leading to the formation of microbialites (Platt and Wright 1991; Arp et al. 2003; Dupraz et al. 2004; Glunk et al. 2011; De Mott et al. 2020).

Because the genesis of microbialites is directly related to environmental settings, they can be valuable tools for paleolimnological reconstructions (e.g., Hillaire-Marcel and Casanova 1987; Talbot 1990; Casanova and Hillaire-Marcel 1993; Arenas et al. 1997; Cohen et al. 1997; Martin-Bello et al. 2019), recording in distinct scales of observation, lake-level fluctuations, paleohydrology, and water chemistry changes. However, although the generating processes of microbialites are exhaustively investigated (see Riding 2000; Dupraz et al. 2009), studies regarding sub-meter-scale correlations on ancient microbialites in marine or nonmarine environments are relatively scarce (e.g., Ibarra and Corsetti 2016; Bunevich et al. 2017; Martin-Bello et al. 2019). Moreover, the formation of microbialite fields where their textural attributes are

directly correlatable seems to be an unusual event, with very few documented occurrences throughout geologic history (e.g., Choudhuri et al. 2016; Ibarra and Corsetti 2016).

The Aptian Crato Member (Santana Formation) of the Araripe Basin is considered an excellent example of a mixed siliciclastic–carbonate paleolake, known chiefly for its outcrops of fine-grained laminated limestones bearing well-preserved fossiliferous content, which has received considerable attention over the last few decades (e.g., Grimaldi 1990; Carvalho and Viana 1993; Mohr and Eklund 2003; Makarkin and Menon 2005; Martill et al. 2007a; Báez et al. 2009; Figueiredo and Kellner 2009; Carvalho et al. 2019; Varejão et al. 2019; Ribeiro et al. 2021), being recognized as a Konservat-Lagerstätte. However, the main characteristics of the depositional environment of this lithostratigraphic unit are still a matter of debate. Multiple sedimentary models have been proposed based on studies which suggest different degrees of salinity of the lake waters (Mabesoone and Tinoco 1973; Neumann 1999; Martill et al. 2007b; Varejão et al. 2019), where a connection with seawater at some stage is proposed (Santos 1982; Arai 1999; Martill 2007; Varejão et al. 2021; Ribeiro et al. 2021). More recently, debates concerning the influence of microbial mediation on the precipitation of the Crato Member limestones have also flourished (Heimhofer et al. 2010; Catto et al. 2016; Warren et al. 2017).

The present study documents a specific laminae succession, initially distinguished by its remarkable textural similarity in far-distant sites of the Araripe Basin. Detailed multiscale characterization and geochemical analysis were employed to investigate the processes and the paleoenvironmental conditions that triggered its widespread and laterally highly uniform deposition. Our results provide new insights into how regional and local sedimentary controls affected the precipitation of this extensive microbialite field, helping to elucidate the development of this kind of feature over large areas in a relatively short period. Additionally, due to the recognition of the deposition of this stratum as a response to a unique and basin-wide geologic event, we here assign the studied interval as a new marker horizon of the Araripe Basin.

GEOLOGICAL SETTING

Structural Framework

The Araripe Basin covers an area of nearly 9000 km², and is the largest with the best preserved stratigraphic record of all the interior basins of northeastern Brazil (Fig. 1). Its genesis is related to the rupture of the Gondwana paleocontinent and the opening of the South Atlantic Ocean, a process initiated in the Barremian with lithospheric stretching, which reached its climax during the Aptian (Matos 1992, 2000). At least in its initial formation stages, the Araripe Basin can be classified as a pull-apart basin with a complex structural framework (Silva 1983, Miranda et al. 2014). It is located in the Transversal Zone of the Borborema Province and is bounded by the Patos and Pernambuco shear zones, with an E–W trend. Also, many NE–SW-trending faults inherited from Borborema Province Proterozoic structures affect the basin (Brito-Neves 1990; Ponte and Ponte Filho 1996), contributing to an architecture based on half-grabens and horsts observed by Ponte and Ponte Filho (1996) and later verified by aeromagnetic surveillance (Camacho and Sousa 2017; Araújo et al. 2019).

Stratigraphy and Marker Horizons of the Araripe Basin

Four sequences constitute the stratigraphic record of the Araripe Basin (Assine 2007). The lowermost stratigraphic sequence was deposited in the Paleozoic (Devonian–Silurian) and is composed of the fluvial sandstones of the Mauriti Formation. The Jurassic lacustrine and fluvial deposits of the Brejo Santo and Missão Velha Formations overlie the Paleozoic sediments and compose the pre-rift sequence. The presence of a new unconformity (based on ostracod content) marks the deposition of the rift

supersequence, which consists in fluvial to lacustrine strata of the Abaiara Formation and was deposited during Berrasian and Hauterivian ages. Two sequences compose the basin's post-rift phase sedimentary stacking. The post-rift I sequence, which is of Aptian age and caps the underlying sequence in angular unconformity, is formed by the fluvial to lacustrine Rio da Batateira Formation (*sensu* Ponte and Appi 1990) and the more complex Santana Formation, described in the following paragraph. Capping the basin sedimentary infill, the post-rift II sequence is represented by Araripina (*sensu* Assine 2007) and Exu formations, with deposition attributed to the Albian and Albian–Cenomanian ages, respectively. This fossiliferous-content dating, however, is still controversial (Regali 2001; Martill et al. 2021).

The Santana Formation (Beurlen 1962) has the most varied lithostratigraphic record of the Araripe Basin, reflecting the evolution of distinct depositional environments: from freshwater to a brackish lacustrine system, represented by the Crato Member, composed mainly of the interdigitation of lutites, laminated limestones, and sandstones (Neumann 1999; Heimhofer et al. 2010); following was the onset of a sabkha lake, with precipitation of gypsum and anhydrite layers that chiefly constitutes the Ipubi Member (Silva 1988; Bobco et al. 2017; Duarte and Borghi 2018); next, a shallow marine system with two transgressive to regressive cycles covered the basin, represented by the Romualdo Member, which is composed of marls, shales, sandstones, and coquina beds (Mabesoone and Tinoco 1973; Custódio et al. 2017; Kroth et al. 2021).

Stratigraphic horizons, eventually formalized as lithostratigraphic units, have more than once been recognized in the Aptian sedimentary record of the Araripe Basin. Being an easily discernible shale to nodular limestones layer among the sandstones of the Rio da Batateira Formation, the Fundão Member (Hashimoto et al. 1987; Rios-Netto et al. 2012) is the first horizon documented and marks the onset of an extensive lacustrine system in the basin (Chagas et al. 2007; Rios-Netto et al. 2012; Fambrini et al. 2016). Recently, Varejão et al. (2020) proposed a new unit in the Crato Member based on lithologic and paleontologic similarities seen in four kilometers distant sites in the east of the Araripe Basin. The so-called Caldas Bed is positioned right above the first package of laminated limestones of the Crato Member, related to a transition from a hypersaline lake to a freshwater system (Varejão et al. 2020, 2021).

MATERIAL AND METHODS

The initial recognition of the studied interval was possible through the analysis of photographic archives and rock descriptions of well cores (IPS-09-CE and IPS-11-CE, from now on called “PS9” and “PS11,” respectively) drilled by CPRM (Geological Survey of Brazil: Santana Project II; Scheid et al. 1978). The identification of a distinct and correlatable lamination pattern among the first-deposited limestones of the Crato Member was possible based on this material. This specific structure is also observed in the outcrops of the Batateira Creek, positioned around the same stratigraphic level (topographic level of 550–600 m; see Fig. 1). Seeking to recover a weathering-unscathed sample of this rock stratum, a short (2.07 m) well core was obtained directly from a limestones outcrop in the Cascata region, on the outskirts of the Crato municipality (Fig. 2). This new core (2-CH-1-CE, here referred to as the “CH core”) is equivalent to the 86.6–88.9 m range of the Rio da Batateira section represented in Figure 3.

A new well core (2-AB-1-CE, here referred to as the “AB core”) was acquired in the Serra da Mãozinha region, a local inselberg. The AB well core recovered over 420 m of continuous record and comprises all the documented lithostratigraphic units of the post-rift sequences. The target layer occurs in this well core between depths 201.5 and 202 m.

The sedimentary attributes of the Crato Member were described in a high-resolution scale (1:40) considering attributes like grain size, sedimentary structures, fossil content, and rock color (based on Munsell Color (Firm)

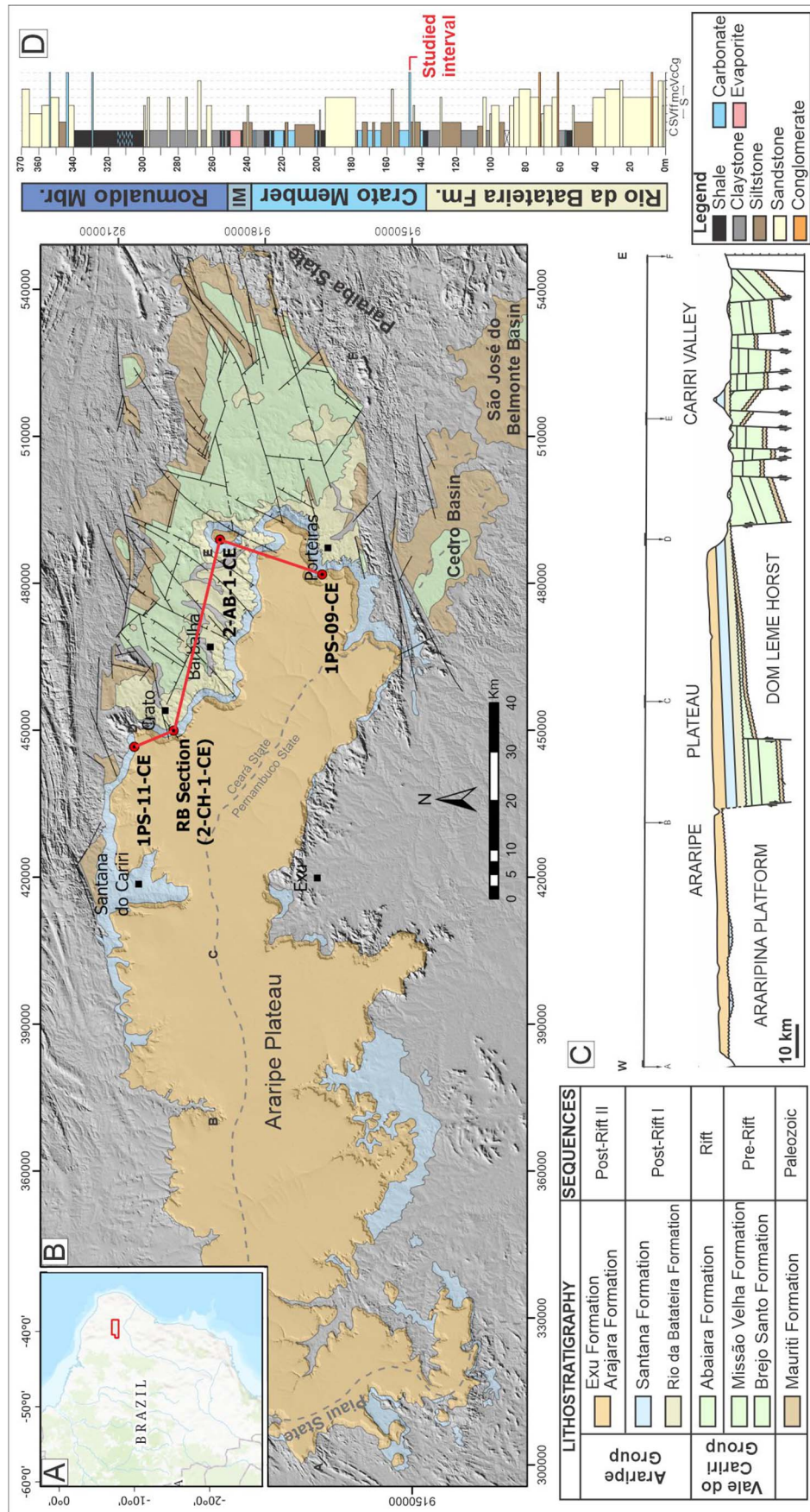


FIG. 1.—Map of the Araripe Basin and its main stratigraphic features (modified from Assine 2007). **A**) Location of the Araripe Basin. **B**) Geologic map of the Araripe Basin with the location of the studied well cores and outcrop. **C**) Geological cross sections across the Araripe Basin, as indicated in Part A. **D**) Representative lithostratigraphic column of the Alagoas Stage strata. IM, Ipubi Member.



FIG. 2.—Overview of Batateira Creek at the laminated limestone outcrops at the Cascata location, with “X” marking the exact spot where the CH core was drilled.

2009) in those four locations as mentioned earlier, all in the eastern region of the Araripe Basin.

Twenty-two samples were collected in the AB and CH cores for petrographic investigation of the interval encompassing the transition between organic shales, nodular limestones, and thinly laminated limestones. Also, a thin section located in the aimed interval (136.30 m) of PS11 core was recovered from the lithologic archive of the Sedimentary Geology Laboratory, Federal University of Rio de Janeiro (LAGESED-UFRJ). The thin sections were prepared and impregnated with blue epoxy resin. All the samples were described and photographed using a Zeiss Imager A1 microscope.

Semiquantitative estimation of the composition of the studied interval was possible using an XRF handheld analyzer (Delta Premium analyzer from Olympus Innov-X). Portable XRF devices provide fast, nondestructive, and reliable means to measure the relative variations of major elements in

carbonate rocks, as long as the necessary calibrations are taken (Sinneasel et al. 2018). Also, since the studied samples come from well cores, the possible effects of weathering on the composition of these deposits can be ignored (Quye-Sawyer et al. 2015).

The instrument uses energy-dispersive X-ray fluorescence technology and is equipped with a Rh anode (maximum parameters: 50 kV, 100 A, 4 W) and a 10 mm² X-Flash[®] Silicon Drift Detector (SDD). The limits of detection (in ppm) for the analyzed elements are: Ca (15), Si (200), S (45), Fe (5), Mn (5), Sr (1), Al (350), P (40), K (20), and Pb (2) (Olympus VANTA). The limits of detection represent the calculated value using a three-sigma 99.7% confidence level. The average standard error found for the elements is < 0.01 for S, K, P, and Sr and < 0.06 for Si, Ca, Mg, and Fe. We obtained seventy readings from the CH core and 51 from the AB core, with a maximum distance of 3 cm from each other and 120 s reading

time for each target spot. Data management, analysis, and representation were performed using Pandas and Matplotlib libraries for Python 3.7 (Hunter 2007; The Pandas Development Team 2020).

Eight carbonate powder samples from each AB and CH cores were sent to the LES laboratory of the University of São Paulo (USP) for carbon and oxygen stable isotopes analysis. A DELTA V Advantage mass spectrometer (equipped with a Gas Bench II Thermo) was calibrated using the NBS18 and NBS19 standards. Results on carbon and oxygen stable isotopes are expressed by a conventional notation relative to the Vienna Pee-Dee Belemnite (VPDB) standard, with a precision of 0.05‰ for $\delta^{13}\text{C}$ and 0.07‰ for $\delta^{18}\text{O}$. In addition, previously published carbon and oxygen isotopic data were compiled (data from Neumann 1999 and Rodrigues 2015) from samples collected at the same studied interval in the PS11 core for comparison purposes.

RESULTS

Mesoscale and Microscale Characterization

F5-6 Three distinct lithotypes compose the studied interval, where the ~ 0.4 m-length nodular limestone is the most easily recognizable. These nodular limestones directly overlie a thinner (~ 0.1 m) layer of organic shales (Fig. 4) and are overlain by a thicker (about 3 m in the AB core) layer of thinly laminated limestones. Description and comparison of the defined basal boundary (P0) and nine overlying laminasets (A to I; sensu Campbell 1967) of the AB and CH cores and photographic records of the PS09 and PS11 cores (in Scheid et al. 1978) allowed a high-resolution correlation between the samples (Fig. 4). Figures 5 and 6 contain a visual summary of the overall characteristics of the studied interval in mesoscale and microscale.

The term “nodular texture” refers to the texture of some carbonates that, when observed in mesoscale (hand sample), are composed of multiple rounded to irregularly shaped nodules associated with a wrinkly irregular lamination, as seen in the laminasets B to F. For these same nodules, in microscale, we adopt the term “clot,” which gives the “clotted fabric” (see Riding 2000; also referred to as “structure grumeleuse” by Cayeux 1935), which is characterized by containing visible microcrystalline peloids, among other particles, surrounded by microcrystalline calcite. This nomenclature is here adopted to avoid misunderstandings with the term “mesoclots,” proposed by Shapiro (2000) and commonly related to nonlaminated thrombolites.

P0.—A millimetric horizon (here named P0) marks the lower boundary of the studied interval. It is characterized by what seems, in mesoscale, an abundance of lamination-oriented, slightly elongated carbonate nodules. A microscopic investigation reveals that the clots are either irregular or spherical to ellipsoidal and range in size from 0.2 to 2 mm, with composition given mainly by microcrystalline calcite but with significant pyritization. It is also possible to observe spherulitic calcite aggregates inside some clots. Besides, these clots can coalesce to the point of forming laminae or be isolated from each other in the dark organic matrix (Fig. 7A).

Laminaset A.—This comprises most of the lithotype here described as organic shale. It consists of black-to-brown, organic matter-rich matrix and typically disarticulated, flattened ostracod valves, often concentrated to form horizontal lenses (Fig. 7B). Ellipsoidal to spherical centimetric to millimetric nodules also occur less commonly in the interval, with its components occasionally displaying diagenetic calcite with spherulitic extinction (Fig. 7C). The laminaset gets darker towards its base, finally reaching P0.

Laminaset B.—Intercalation of relatively thick light calcitic (about 2 to 4 mm) and dark organic laminae (about 1 to 2 mm) in a wrinkly pattern is the main attribute of Laminaset B. The ubiquitous dark laminae of the studied interval are of organic origin (bacterial strands) as evidenced in

Figure 8A and B. Clotted fabric defines the calcitic laminae (Fig. 7D), where it is possible to discriminate distinct components inside the clots like peloids and calcitic spheroids (Fig. 8C, D). Also notable is a sinuous arrangement inside some intraclasts, with a possible origin related to cementation adjacent to bacterial filaments. Often, millimetric, irregularly shaped intraclasts composed uniquely of spherulitic calcite appear in this laminaset, usually associated with the dark organic laminae. These organic laminae also contain disarticulated ostracod valves, like those seen in Laminaset A. Centimetric spherical intraclasts occasionally enclose phosphatic organic remains (probably fish bones) and are likely to be more likely to appear in this laminaset (Fig. 7E). Features related to dissolution, cementation, and replacement by chalcedony, microcrystalline silica, and macrocrystalline calcite are apparent in this laminaset in both the CH and AB cores, where either the calcitic laminae and the interior of the articulated ostracod valves are affected. Additionally, it is often possible to find centimetric carbonized plant remains in this laminaset.

Two laminae composed of peloids and ostracod valves separated by centimeters from each other are a key marker at the base of Laminaset B, clearly visible in both the CH and AB cores (Fig. 7F).

Laminaset C.—The nodular limestones of Laminaset C are distinguishable in mesoscale by abrupt dark organic laminae thinning when compared with the adjacent laminasets, with also clot-coalesced laminae where cementation and/or replacement is often observable. The features related to dissolution, cementation, and replacement by chalcedony, microcrystalline silica, and macrocrystalline calcite observed in Laminaset B are also present in this laminaset (Fig. 7G, H).

Laminaset D.—Intercalation of nodular and thinly laminated fabrics, outlined by dark organic laminae with variable thickness, are the most prominent features of Laminaset D in mesoscale. The thin carbonate laminae are, in fact, continuous and represent sub-sets marked by clot-coalesced fabrics, with recurrent-thickness laminae (about 1 mm) (Fig. 9A). Well-defined, individualized clots occur at the bottom and top of this laminaset. Clots composed entirely of calcite spherulites also appear associated with the bottom most dark organic laminae near the boundary with Laminaset C.

Laminaset E.—Laminaset E can be characterized in mesoscale as an interval of nearly 10 mm consisting of limestones with an almost incipient lamination. Petrographic analysis reveals that it is composed of thin, presumably clot-coalesced laminae similar to the ones seen in Laminaset D, where here they generally have a greater thickness and no defined pattern (Fig. 9B). Dark organic laminae are indeed very thin and sometimes discontinuous. Ostracod valves are also relatively abundant in this laminaset, as they occur predominantly disarticulated. Rare irregular nodules composed of spherulites may also be present.

Laminaset F.—The main textural feature of Laminaset F is its nodular fabric, where subtle changes are noticeable. The most recognizable microscale characteristics of this laminaset are: 1) laminae dominated by well-defined clots, 2) nearly planar clot-coalesced laminae, and 3) dark organic laminae with variable thicknesses (Fig. 9C). Inside many clots, a sinuous arrangement is also observable (Fig. 9D), which is tentatively related to bacterial filaments (see Discussion). The presence of clots composed solely of calcitic spheroids, a recurrent feature of the whole studied interval, is much more common in this laminaset (Fig. 9E). Bedding-parallel fibrous veins (beef structures), which are commonly related to fluid overpressure (Cobbold et al. 2013), are often present towards the top of this laminaset in the AB core (Fig. 9F). This feature is nearly absent in the CH and PS11 cores, representing post depositional differences between the rock records. The upper boundary of this

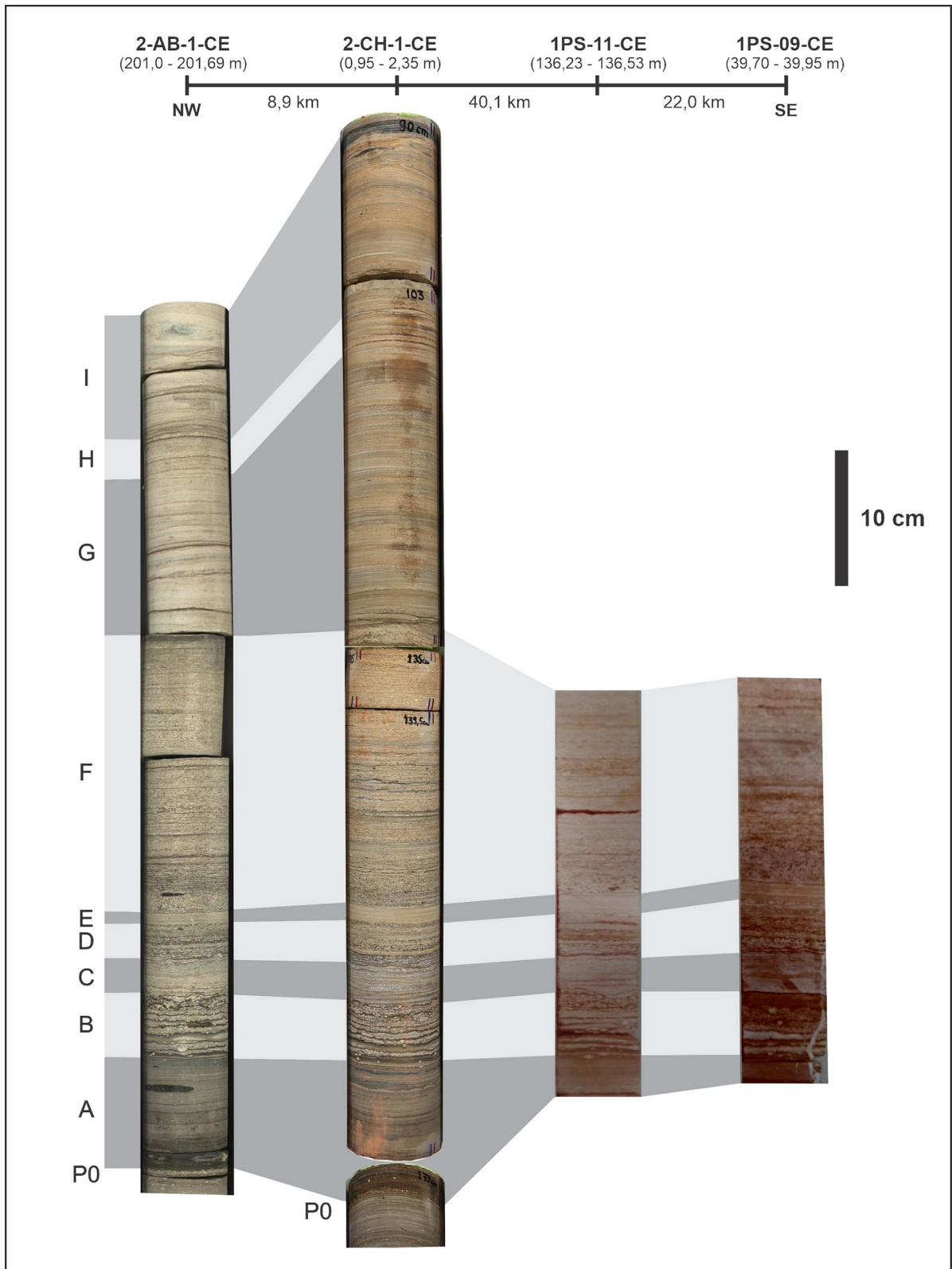


FIG. 4.—Comparison of the studied interval, with its respective depth in different well cores, featuring the laminasets defined here. Photographs of the PS09 and PS11 cores are reproduced from Scheid et al. (1978).

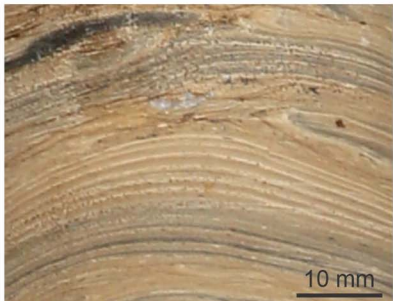

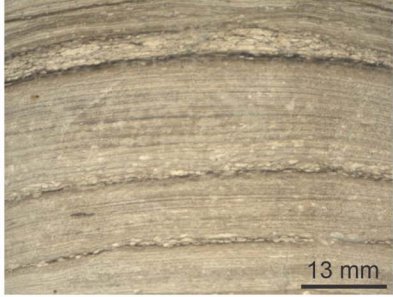
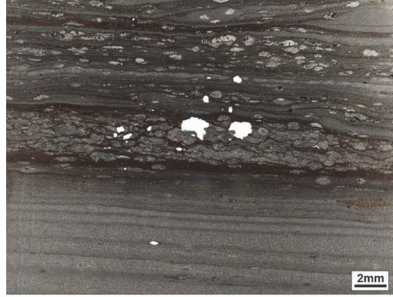
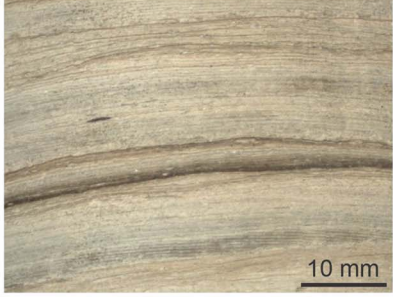

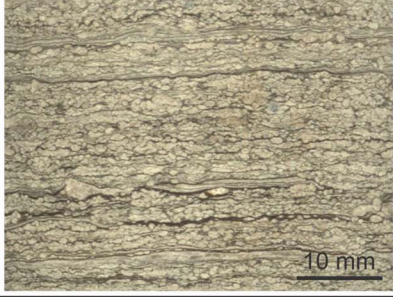

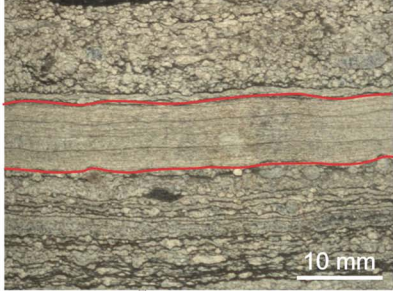
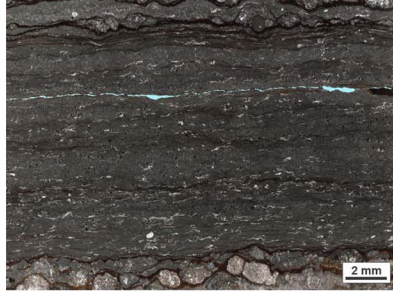
Lst	Mesoscopic characterization	Microscopic characterization
I	 <p data-bbox="703 285 810 449">Thinly laminated limestones with centimetrical slumps and loop beddings.</p>	 <p data-bbox="1235 306 1328 470">Mudstone with lamination evidenced by color rhythmic alternation (//P).</p>
H	 <p data-bbox="703 604 810 768">Thinly laminated limestones with a triplet of nodular limestone laminae.</p>	 <p data-bbox="1235 604 1328 810">Alternation of laminae composed by microcrystalline calcite and clotted fabric laminae (//P).</p>
G	 <p data-bbox="703 913 810 1077">Thinly laminated limestones with occasional dark organic laminae and slumps.</p>	 <p data-bbox="1235 871 1328 1119">Mudstone with rhythmic lamination. Isolated millimetric dark organic laminae also occur. Loop beddings are often distinguishable (//P).</p>
F	 <p data-bbox="703 1201 810 1415">Nodular limestones, with irregularly intercalation of two types of carbonate laminae and dark organic laminae.</p>	 <p data-bbox="1235 1180 1328 1436">Clotted fabric limestone, with lamination given by intercalation with organic laminae. Calcite cementation is often visible (//P).</p>
E	 <p data-bbox="703 1488 810 1745">Very fine grained limestones, with submillimetric dark laminae. The upper and lower limits of the laminaset are highlighted in red.</p>	 <p data-bbox="1235 1509 1328 1703">Clotted laminae. Disarticulated and deformed ostracod valves occur sparsely (XP).</p>

FIG. 5.—Mesoscale and microscale characterization of the laminasets E to I. Lst, Laminaset. //P, uncrossed polarizers; XP, crossed polarizers.

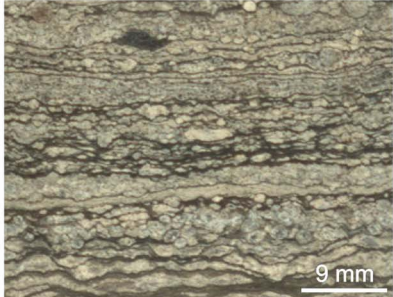


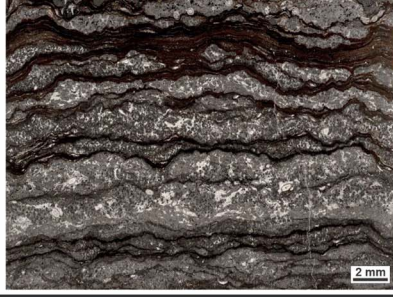
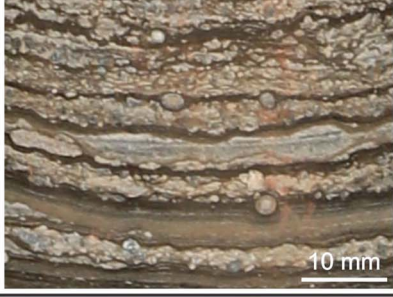
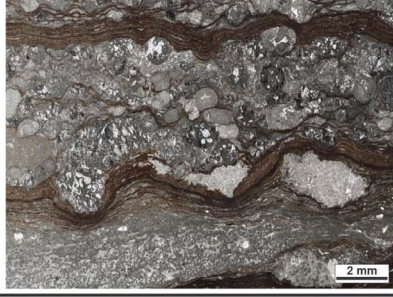
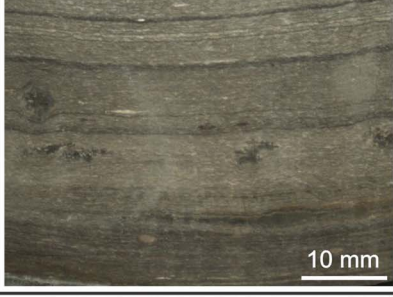

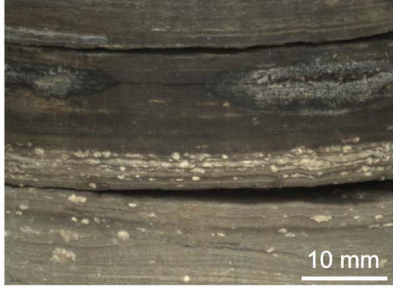
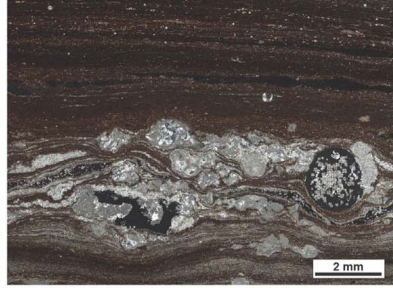
Lst	Mesoscopic characterization	Microscopic characterization
D	 <p>Nodular limestone with irregular lamination given by intercalation with millimetric dark laminae.</p> <p>9 mm</p>	 <p>Calcitic laminae with distinctly-arranged clotted fabrics. Dark organic laminae also display thickness variation (XP).</p> <p>1 mm</p>
C	 <p>Nodular limestone, with lamination given by intercalation with submillimetric dark organic laminae. Cementation is often visible.</p> <p>9.2 mm</p>	 <p>Calcitic laminae given by stretched clots with visible cementation given by macrocrystalline calcite (//P).</p> <p>2 mm</p>
B	 <p>Wrinkly laminated nodular limestone. Spherical nodules often occurs.</p> <p>10 mm</p>	 <p>Flat peloidal and irregular clotted fabric laminae alternating with relatively thick dark organic laminae (//P).</p> <p>2 mm</p>
A	 <p>Organic shale with darkening trend towards the base. Carbonized plant remains are often visible.</p> <p>10 mm</p>	 <p>Organic shale with abundant ostracod valves. These bioclasts are disarticulated and compacted (//P).</p> <p>0.5 mm</p>
P0	 <p>Dark shale containing a horizon marked by oriented carbonate nodules.</p> <p>10 mm</p>	 <p>Calcitic laminae given by coalesced, spherical and elliptical clots. Spherulitic calcite is also visible inside some clots (XP).</p> <p>2 mm</p>

Fig. 6.—Mesoscale and microscale characterization of the laminasets P0 to D. (Lst, Laminaset; //P, uncrossed polarizers; XP, crossed polarizers).

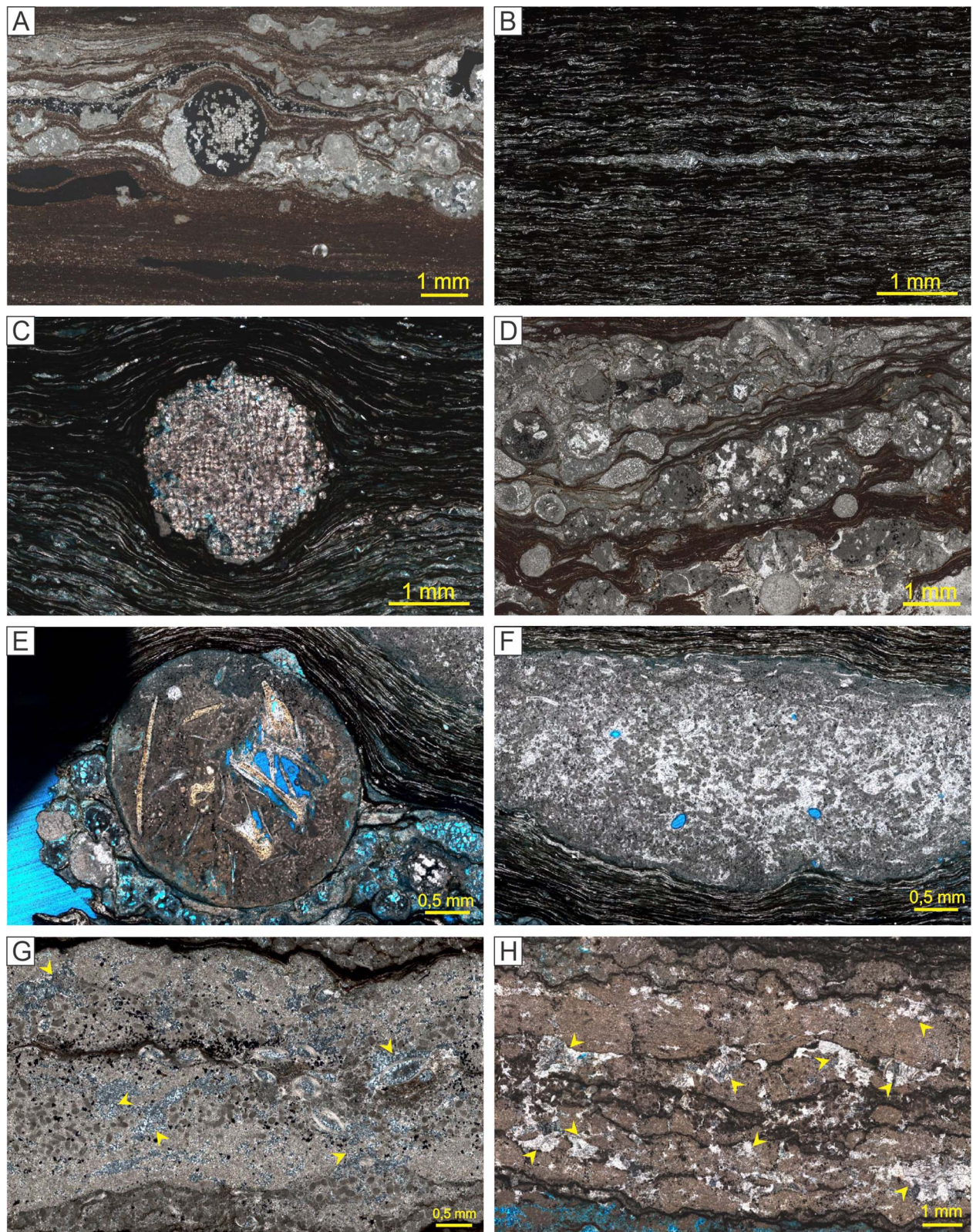


FIG. 7.—Photomicrographs of laminasets (Lst) features. **A**) P0, contact between the organic shale and calcitic clotted laminae; restricted, yet intense pyritization affects either calcitic laminae and the spheroidal clot in the center of the image, where spherulites can also be observed (XP). **B**) Lst A, organic shale with abundant flattened and disarticulated ostracod valves (//P). **C**) Lst A, diagenetic nodule inserted in an organic matrix mainly composed of spherulites (XP). **D**) Lst B, clotted fabric of calcite laminae (//P). **E**) Lst B, spheroidal intraclast containing calcitic to phosphatic material possibly related to fish bones (//P). **F**) Lst B, peloidal calcitic lamina, with sparse ostracod valves (//P). **G**) Lst C, peloidal calcitic lamina with local substitution by silica, as indicated by the yellow arrows (XP). **H**) Lst C, peloidal to microcrystalline–cryptocrystalline calcitic lamina with pores filled by macrocrystalline calcite indicated by the yellow arrows (//P).

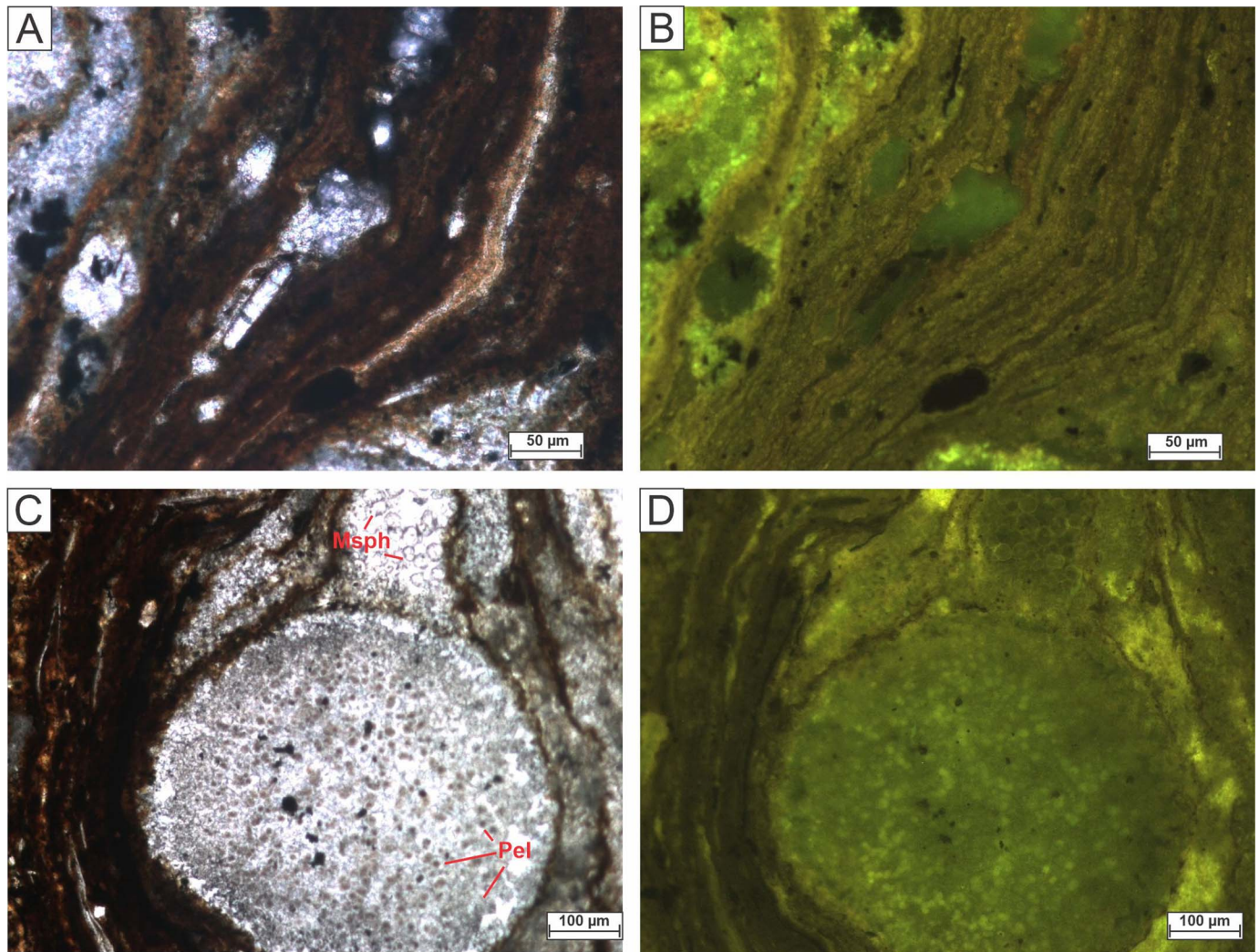


FIG. 8.—A, C) Transmitted white light and B, D) fluorescence mode images of calcitic clots and dark laminae of Laminaset B. The ubiquitous dark laminae of the studied interval, like the ones seen in Parts A and C, are of organic origin (bacterial strands), as evidenced in Part B. Also, as further outlined in Parts C and D, peloids (Pel) and calcitic spheroids (Msph) are common constituents of clots.

laminaset also marks the end of deposition of the continuous nodular limestones.

Laminaset G.—Laminaset G, the first of the thinly laminated limestones, occurs with an abrupt contact with the underlying laminaset, often marked by slumps or loop beddings (Bates and Jackson 1980; Calvo et al. 1998). This laminaset shows considerable thickness variations between the AB and CH cores (13 and 23 cm, respectively), with the occasional occurrence of prominent dark organic laminae in the AB core. Petrographic investigation provides evidence that these thinly laminated limestones are mudstones with rhythmic alternation with crystallinity differences and an association with organic matter, evident by the lighter and darker colors of the laminae. Isolated, nearly ellipsoidal clots occur sparsely, commonly deforming the lamination. Thick (1 to 2 mm) isolated dark organic laminae may also appear.

Laminaset H.—The appearance of an aligned-nodules-rich, dark organic lamina marks the transition between the laminasets G and H (Fig. 9G). Laminaset H is composed mainly of thinly laminated limestones, with the aforementioned nodular lamina being the first of a triplet. These

three nodule-rich laminae correspond to narrow reappearances of the clotted fabric characteristics of laminasets C to F (Fig. 5).

Laminaset I.—The most remarkable aspect of the thinly laminated Laminaset I is the moderate to intense deformation of its laminae by soft-sediment deformation structures (SSDS), represented by slumps and loop beddings (Figs. 5, 9H). Also, this mudstone exhibits the same rhythmic lamination created by differences in crystallinity and the presence of organic matter described for Laminaset G.

Compositional Analysis

Ten time series were selected based on abundance in the studied cores and relevance to environmental settings. These pXRF time series include Ca, Si, S, Fe, Mn, Sr, Al, P, K, and Pb, representing typical lake sediments, where the first five listed together sum up nearly 98% of total detectable rock composition along both cores. Also, these elements are useful as proxies for processes that affect the depositional setting, like detrital input, lake water oxygenation, and biological production in lakes and other environments (Cohen 2003; Davies et al. 2015; Herndon et al. 2018). Figure 10 illustrates the variations of element

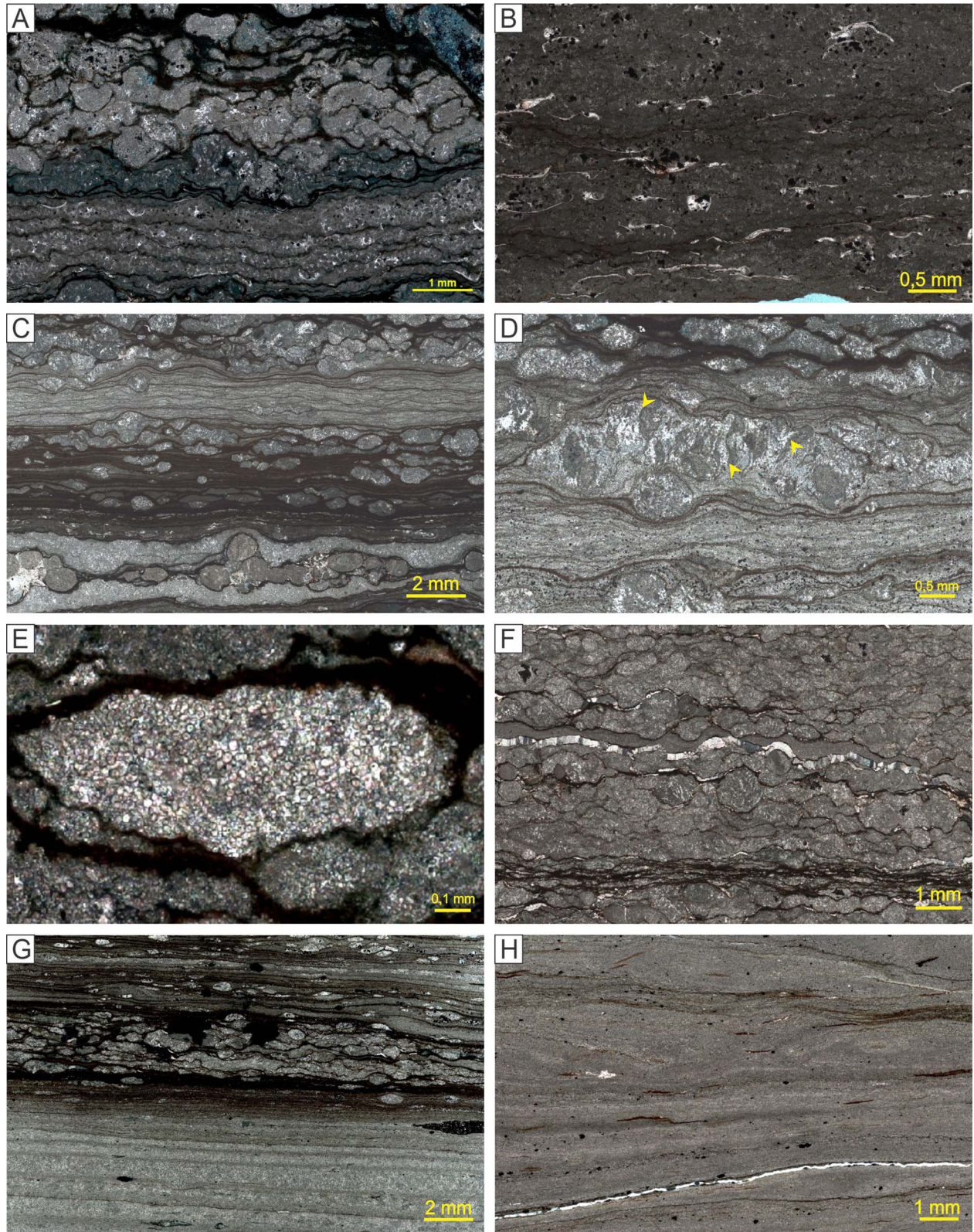


FIG. 9.—Photomicrographs of laminasets (Lst) features. **A**) Lst D, interface between underlying peloidal laminae and overlying clotted laminae (XP). **B**) Lst E, nearly indistinguishable clot-coalesced laminae with sparse disarticulated ostracod valves (XP). **C**) Lst F, intercalation of well-defined clots associated with dark organic laminae and clot-coalesced laminae (XP). **D**) Lst F, observable inferred subvertical filament molds, indicated by yellow arrows, inside a clot (XP). **E**) Lst F, clot composed mainly of calcitic spheroids (XP). **F**) Lst F, macrocrystalline calcite lens following the general orientation of the limestone (XP). **G**) Lst H, one of the clotted laminae marks the limit of the laminasets G and H (XP). **H**) Lst I, soft-sediment deformation in mudstone (//P).

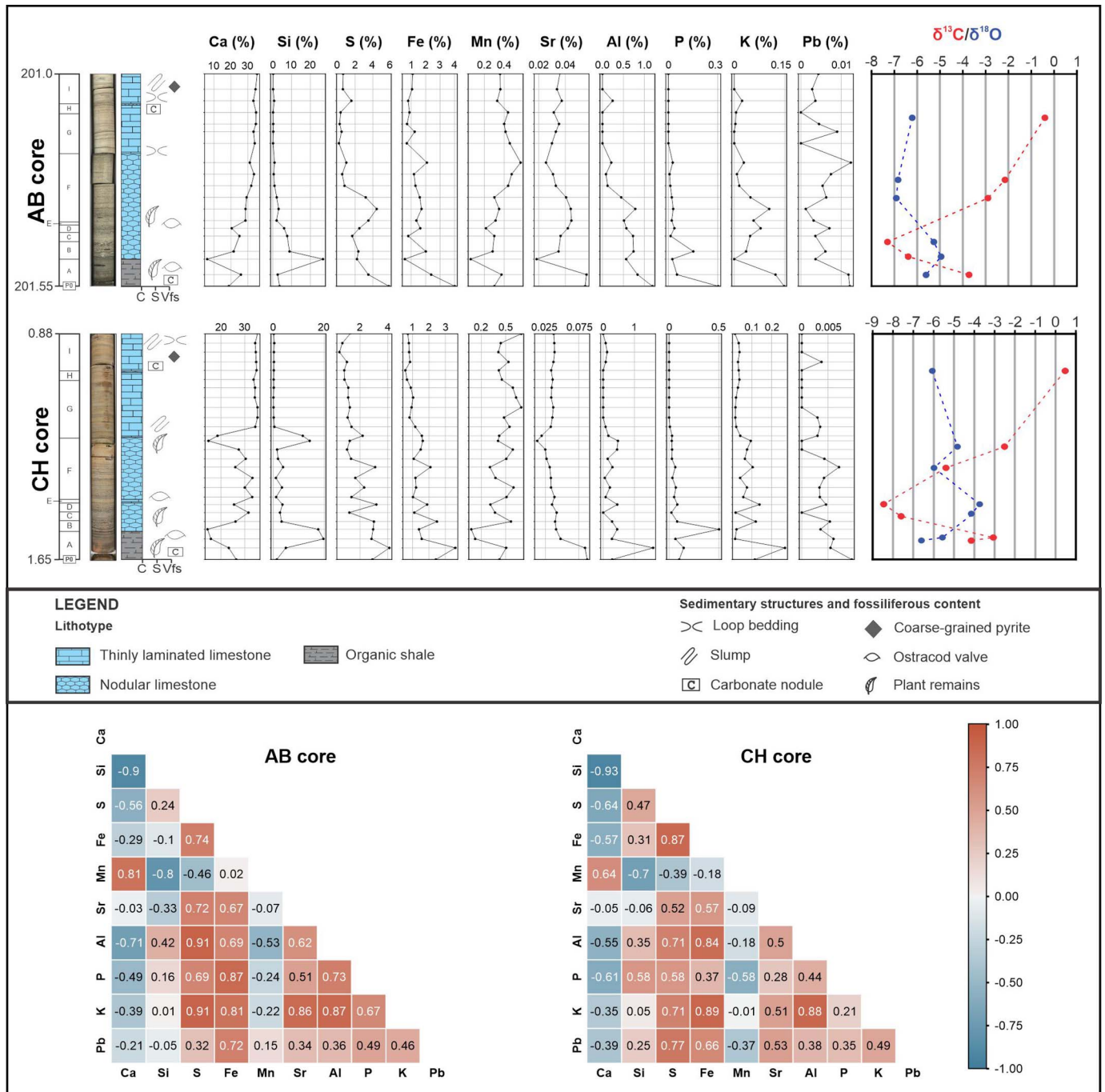


Fig. 10.—Compositional and isotopic variation logs of the AB and CH cores in the study interval, with the respective compositional Pearson correlation matrices.

concentrations (expressed by log curves) and correlation matrices for each analyzed core.

The first observable aspect of the compositional analysis of the studied interval is the predictable negative correlation between the Ca and Si logs, reflecting mainly the lithologic difference between limestones and shales. Nonetheless, positive peaks of Si in Laminaset B of both cores are also observable, as a the Ca increase and Si decrease in the transition between nodular limestones and laminated limestones in the CH core.

Aluminum contents are moderately correlated with Si in both cores, following a decreasing-upward trend and roughly finding its peaks in the

same heights of the Si log. However, despite showing strong, nearly identical correlations with Al in both cores, the K contents do not suggest any correlation with Si. Still, the Al logs also tend to express strong positive correlations with Fe and S.

The sulfur contents in both cores find their highest values in the organic shales of Laminaset A, with a more or less evident decreasing trend towards the top of the studied interval. Fe contents are positively correlatable with S, which is probably related to the observed widespread pyritization of the original components throughout the interval. It is also noteworthy that the Fe quantities in the AB core show much more variation than that seen in the CH core. This

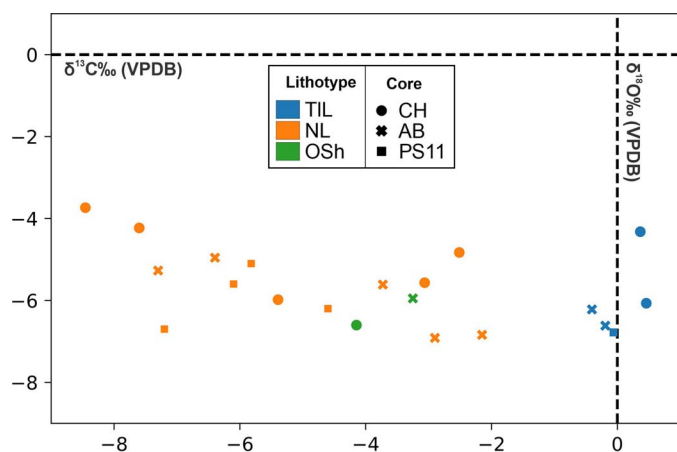


FIG. 11.—Plot of $\delta^{13}\text{C}$ and $\delta^{18}\text{O}$ of the study interval in the CH, AB, and PS11 cores, with lithotype discrimination. TIL, thinly laminated limestones; NL, nodular limestones; OSh, organic shales.

phenomenon is also observed in the analysis of Mn quantities of both cores, although no clear correlation is observable between Fe and Mn in the studied interval. On the other hand, Mn concentration logs again seem to be in a good correlation with the Ca variations in the AB core, indicating the presence of this element in calcites, commonly as a replacement of Ca.

Pb shows moderate to high correlations with Fe and S and is probably related to the content of this element in pyrite crystals, with a highly erratic behavior throughout the studied interval in both cores.

It is noticeable that P contents tend to be higher in the bottom organic shales, with a pronounced decrease throughout the overlying limestones. A strong correlation (0.87) of this element with Fe is attestable in the AB core. Strontium finds its highest values, both in AB and CH cores, in the organic shales of Laminaset A, showing a strong positive correlation with K in the AB core.

Stable-Isotope Analysis

Light values of $\delta^{13}\text{C}$ and $\delta^{18}\text{O}$ are predominant throughout both the AB and CH cores, with different degrees of variability for each stable-isotope ratio investigated (Fig. 10).

In both cores, the $\delta^{13}\text{C}$ shows marked variability, with values ranging between -8.45 and 0.46‰ in the CH core and between -7.30 and -0.19‰ in the AB core. It is also possible to observe a substantial decrease in the $\delta^{13}\text{C}$ values at the point that would correspond to the lower half of the nodular-limestone interval (between laminasets B and E), where its minimum marks are reached. The $\delta^{13}\text{C}$ values increase upwards, reaching more positive marks at the top of the studied interval within the thinly laminated limestones (Fig. 10).

The $\delta^{18}\text{O}$ values present less variability, ranging between -6.60 and -3.73‰ in the CH core and -6.91 and -4.95‰ in the AB core. The $\delta^{18}\text{O}$ more positive values correspond to the samples where the $\delta^{13}\text{C}$ lowest values are observed, with a slight decrease upward in both cores.

Already published stable-isotope data (from Neumann 1999 and Rodrigues 2015) of five samples collected in the nodular limestones and adjacent thinly laminated limestones of the PS11 core are constrained in similar ranges, with $\delta^{13}\text{C}$ values between -7.20 and -0.06‰ and $\delta^{18}\text{O}$ values between -6.78 and -5.10‰ . In this dataset, it is again observable that the $\delta^{13}\text{C}$ values seem related to the lithotypes, with the highest observed value corresponding to the sample collected among the thinly laminated limestones. Figure 11 presents a cross plot including the values of $\delta^{13}\text{C}$ and $\delta^{18}\text{O}$ of all studied cores, where the relation of lithotype and $\delta^{13}\text{C}$ values are readily observable.

DISCUSSION

Microbial Nature of Nodular Limestones and Diagenetic Alterations

Neumann et al. (2003) suggested a microbially related origin for a part or all of the Crato Member limestones. More recently, Catto et al. (2016) reported the existence of several attributes of these rocks that confirm this hypothesis. Either in thinly laminated or in nodular limestones, remnants of calcified microstructures, like honeycombs and spheroids, are related to exopolymeric substances (EPS), coccoidal and filamentous bacteria, indicating organomineralization (Catto et al. 2016). Also, the contribution of microbial mats to the preservation of the fossil content has been the focus of many studies (Barling et al. 2015; 2020; Osés et al. 2016; Varejão et al. 2019; Dias and Carvalho 2020; Iniesto et al. 2021). However, the spatial distribution of these rocks, either vertically or horizontally, is somewhat poorly explored because most of the previous studies are based on samples of few outcrops and well cores, generally restricted to specific intervals and located primarily in the restricted quarry areas of the Araripe Basin.

The nodular fabric, present in laminasets B to F, with rhythmic intercalation of clotted and dark organic (bacterial strands) laminae, is the most readily recognizable attribute of the studied interval and is a common feature related to EPS calcification (Riding 2000; Arp et al. 2003; Dupraz et al. 2004; Riding and Tomás 2006). Based on this textural pattern and the relative scarcity of allochthonous grains in the calcitic laminae, we suggest that *in situ* CaCO_3 precipitation is the most likable process for the formation of the nodular limestones of the study interval.

Calcified remnants of filaments (given by the sinuous and subvertical arrangements observed in some clots, very much like the ones presented by Maisano et al. 2020 in modern microbial mats) and calcitic spheroids, probably related to coccoid cyanobacterial communities such as those described by Perri and Spadafora (2011), were identified. These features indicate an early process of mineralization affecting the bacterial bodies and promoting their fossilization, a process attributed to SRB mediation of carbonate precipitation (van Lith et al. 2003). Conversely, other original components of the microbial communities may also be fossilized by the early calcification process, resulting in different textures. For example, a very similar relationship exists between the clot-coalesced laminae of Laminaset E and the mid-water bacterial mats preserved in black shales described by Oschmann (2000). It is also noteworthy that the occasional alternation of different types of clotted fabrics (e.g., laminae composed of well-defined clots vs. nearly planar clot-coalesced laminae of Laminaset F; see Fig. 9C) may be directly related to the episodic variation of carbonate precipitation mechanisms (i.e., autochthonous precipitation vs. trapping and binding) and distinct microbial communities original arrangements, where cyanobacterial metabolism could also trigger the main budget of CaCO_3 precipitation (Perri et al. 2012; Suarez-Gonzalez et al. 2014). However, more studies are needed to precisely identify the main bacterial agents involved in the precipitation of each laminaset.

The diagenetic overprints in the studied interval predominantly suggest eodiagenetic conditions. In this sense, it is also noteworthy that most microbial processes related to carbonate lithification are considered part of the modifications of the “eodiagenetic realm” as the first postdepositional crystals are forming (Armenteros 2010; De Boever et al. 2017).

Accordingly, the most common features associated with diagenesis in the studied interval are: 1) calcite lithification and cementation through biomediated processes (Arp et al. 2003; Dupraz et al. 2004; Armenteros 2010), 2) scattered occurrence of framboidal microcrystalline pyrites, randomly replacing components in both organic shales and nodular limestones, associated with reducing conditions and presumably related to interactions sulfate-reducing bacteria with organic matter (Berner 1985; Dupraz et al. 2004; Duverger et al. 2020), 3) localized dissolution of peloids and cementation as macrocrystalline calcite, and 4) sparse silicification of localized clots (in laminasets B and C), which can be related to silicic acid-binding on microbial surfaces (Renaut et al. 1998; Bustillo 2010).

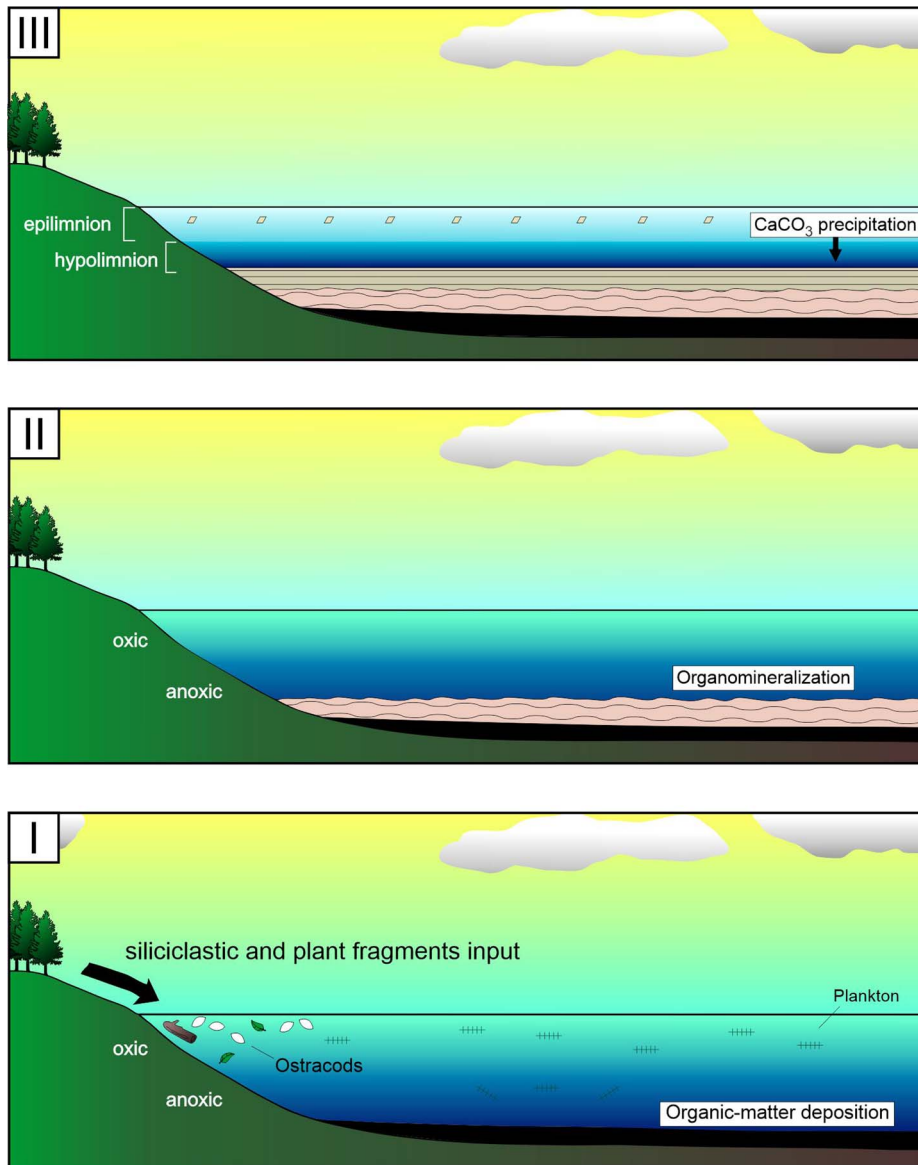


FIG. 12.—Simplified depositional model of the lithotypes that constitute the studied interval. I) Organic-shale deposition with a large contribution of organic matter and disarticulated ostracod valves. Anoxic settings would already be prevalent. II) Biologically induced mineralization (organomineralization) of stromatolites under anoxic conditions and with lower rates of water input. III) Deposition of laminated limestones from the precipitation of calcite crystals formed in the epilimnion of a stratified lake.

Finally, the nearly parallel, well-defined lamination and the proven benthic microbial deposition allow classification of the microbialites of the study interval as stratiform, peloidal stromatolites (Kalkowsky 1908; Riding 1999; Flügel 2010).

The apparent abrupt shift that marks the end of stromatolite development and the onset of deposition of thinly laminated limestone can also represent a change in the lake's main processes of CaCO_3 precipitation. Instead of precipitation directly conditioned by the metabolism of bacteria which constitutes microbial mats present in the lake substrate, the formation of calcite microcrystals that make up the laminated limestones is considered to have occurred in the pelagic zone, with planar lamination dictated by seasonal controls ("whiting" events; Kelts and Hsü 1978). Biological influence would still be present in carbonate precipitation but would be related to planktonic activity, a hypothesis also raised by Heimhofer et al. (2010).

Paleoenvironmental and Paleodepositional Insights

Petrographic and geochemical data of both well cores indicate variations among the three analyzed lithotypes, reflecting changes in paleoenvironmental and genetic processes during their deposition.

Organic shales are the first deposited lithotype of the studied succession. Besides the presumably high contents of organic matter, an abundance of disarticulated ostracod valves and sparse carbonate intraclasts are also observable. Enrichment and preservation of organic matter are commonly related to high primary production allied to dysoxic to anoxic environments, where the rate of organic-matter accumulation must be higher than the rate of the combined effects of decay by microbes and dilution by clastic and carbonate sediments (Bohacs et al. 2000; Renaut and Gierlowski-Kordesch 2010). As long as the source of organic matter may be autogenic, allogenic, or a combination of both, the centimetric plant fragments found in both cores give evidence that allogenic contribution was present, but it is inferable that the lithotype also had autogenic organic-matter precipitation. The existence of an anoxic bottom, limiting scavenging and the activity of bacterial respiration, favors the preservation of organic matter (Bohacs et al. 2000).

In both studied cores, it is observed that the relative increase in the peaks of phosphorus correspond to specific laminae of the organic shales immediately below the first nodular limestones. Weathering of phosphate-bearing igneous and sedimentary rocks is the primary source of phosphorus in lakes (Cohen 2003). Its cycle includes delivery from the catchment, storage in the

sediments, and release during anoxic conditions (Corella et al. 2012; Evans et al. 2019), where microbial activity can strongly affect the latter process (Cohen 2003). Therefore, the observed P increases in organic shales suggest a pronounced anoxic setting at least in the bottom waters of the paleolake.

Also, redox transformations govern the chemistry of Fe and Mn in oxic and anoxic waters and sediments, providing information about changing redox conditions in lakes (Davison 1993). Under reducing conditions, Fe and Mn become more soluble, Mn more easily than Fe (Mackereth 1966; Boyle 2001). As such, an increase in the relative quantity of Fe concerning Mn indicate the onset of anaerobic conditions of bottom lake waters of a stratified lake or deoxygenation derived from organic decay following enhanced biological productivity (Davies et al. 2015). In the AB and CH cores, the contents of Fe are much higher than Mn, and no correlation between them is observable. Thus, the values of the Fe/Mn ratio would be higher on the interval comprised by the organic shales (P0 to Laminaset A), pointing to less oxygenated conditions during the deposition of this lithotype.

The poor oxygenation of the lake bottom would also present a hostile environment for most ostracod species, which is not consistent with a large number of valves in this interval. The abundance of ostracods indicates an ostracod bloom, which probably occurred in shallow freshwater with a sudden high nutrient enrichment (Kelts 1988; El Hajj et al. 2021). Nonetheless, this same high nutrient influx would also promote algal or cyanobacterial blooms, which produce lethal toxins and may initiate a mass mortality event (El Hajj et al. 2021). Slow compaction would later promote the disarticulation of the deposited carapaces.

The existence of an environment where ostracods could thrive and even bloom suggests that the waters of the lake were already stratified or beginning to stratify at the time of deposition of the organic shales. However, input of water and detrital sediment, evident by the enrichment of Si, K, and Al and depletion of Ca, would contribute to lake water mixing at this stage. Finally, it is possible to affirm that more humid conditions prevailed in the environment during the deposition of this lithotype, where the paleolake likely received regular fluvial input. This is evident both from the siliciclastic contribution and the aforementioned higher quantity of terrestrial plant fragments.

The deposition of nodular limestones (planar stromatolites) followed the sedimentation of organic shales. The negligible siliciclastic input observed in both nodular and thinly laminated limestones suggests that carbonate precipitation took place in a closed to semi-closed lake characterized by a predominantly arid climate, although occasional rainfall events occurred. The chemical composition of these limestones also reflects the deposition in this environment. Calcium has both allochthonous (erosional) and autochthonous (*in situ* precipitation) sources (Cohen 2003), where source predominance can be deduced by its relationship with strontium (e.g., Kylander et al. 2011; Davies et al. 2015; Evans et al. 2019). The lack of correlation of Ca with Sr and the positive correlations of Sr and typically allogenic elements (K and Al) throughout the carbonates corroborates that autochthonous precipitation was the principal process involved in the formation of the nodular and thinly laminated limestones, with little detrital influence.

Variations of S and Fe, with a positive correlation between these two elements in the analyzed cores, can be associated with the observed early diagenetic framboidal pyrite microcrystals, which replace calcite microcrystals and organic matter in the stromatolites. The formation of microcrystalline framboidal pyrites can be related to high sulfide production as a result of low O₂ contents and high bacterial sulfate-reduction rates in the benthic zone of the paleolake, which would favor porewater FeS saturation, leading to the formation of framboidal pyrite during the first stages of diagenesis (Taylor and Macquaker 2000; Herndon et al. 2018). Also, the average small sizes of the observed pyrites indicate that its formation occurred under euxinic conditions (Wilkin et al. 1996). These observations lead to the assumption that the lake bottom was still poorly oxygenated during the biologically induced mineralization of the stromatolites.

Hypersaline conditions being the most favorable to stromatolite spreading is due to the absence of, in order of importance: 1) algal metaphytes, which would promote competition for light and space and 2) metazoans, which would promote grazing of the microbial mats (Farmer 1992; Des Marais 1995). Therefore, documentation of widespread stromatolite development in saline to hypersaline environments is not uncommon (e.g., Dupraz et al. 2004; Dupraz and Visscher 2005; Vasconcelos et al. 2006; Oliveri et al. 2010; Janhert and Collins 2013). Warren et al. (2017), based on the formation of halite hopper crystals and other salt pseudomorphs in the thinly laminated limestones of the Crato Member (also observed by Martill et al. 2007b), pointed to a shallow-water lacustrine environment as the most likely setting for the deposition of the stromatolite field presented in their study, which is probably located a few meters above the one described here.

However, previously published $\delta^{18}\text{O}$ data (Neumann 1999; Rodrigues 2015) and those presented here for the same interval, indicate light overall values of $\delta^{18}\text{O}$, suggesting that calcite precipitation occurred in a freshwater environment (Leng and Marshall 2004). Heavier $\delta^{18}\text{O}$ values can be observed in the first laminae of the nodular limestones of both cores, possibly indicating the onset of short-lived increased evaporation rates. Nonetheless, this trend is readily reversed to lighter values and is still far below the ones that a saline environment should display, where it is expected to find heavier $\delta^{18}\text{O}$ values due to the loss of ^{16}O to evaporation (Leng and Marshall 2004). Based on this assumption, factors other than the higher rates of evaporation might have acted for a lower discharge of water into the lake during the deposition of carbonates, where the movement of blocks by tectonic action is a plausible hypothesis (Carroll and Bohacs 1999).

Varejão et al. (2021) address the apparent inconsistency regarding the $\delta^{18}\text{O}$ values with a hypersaline lake environment for the lower thinly laminated limestones of Crato Member. These authors point to the possible distorting effects of meteoric diagenesis, which would not nullify the paleoenvironmental interpretations. Although the action of meteoric diagenesis cannot easily be validated or discarded in the studied interval, we did not find any direct evidence of this process either.

Therefore, although numerous studies show that seasonal hypersalinity was a recurrent lake attribute throughout the deposition of the Crato Member's upper thinly laminated limestones, we do not observe any direct evidence of high salinity during precipitation of the stromatolites presented here. Instead, the data support that organomineralization took place in a freshwater, possibly brackish lake.

Several environmental factors control the $\delta^{13}\text{C}$ of dissolved inorganic carbonate (DIC), like changes in atmospheric equilibrium, aquatic photosynthesis, pH of an aquatic environment, and the input of land-plant debris, besides postdepositional processes (Talbot 1990; Zeebe and Wolf-Gladrow 2001; Deocampo 2010). The resulting $\delta^{13}\text{C}$ logs of the studied cores present remarkable similarity and seem strongly conditioned by lithotype. The negative excursion of the bottom laminae of the nodular limestones can be at least partially attributed to the decomposition of the organic matter of the microbial mats that constitutes either the organic shales or the thick dark laminae of the stromatolites. Microbial mats can yield strong negative $\delta^{13}\text{C}_{\text{org}}$ signatures (Schildowski 2000), and the dissolution of this material under anoxic bottom lake waters, releasing ^{12}C into the DIC pool, tends to produce lighter $\delta^{13}\text{C}$ values. On the other hand, the loss of more reactive components of organic matter during the early stages of diagenesis can also explain the negative shift in this interval, because this process can result in much more negative $\delta^{13}\text{C}$ values for organic matter (Cohen 2003). At last, considering the stratified nature of the lake, it is plausible that an ongoing process of methanogenesis at the sediment-water interface could have also influenced the isotopic carbon signature of these rocks (Talbot and Kelts 1986; Cohen 2003).

An increase of $\delta^{13}\text{C}$ values towards the top of the cores partly evidences the end of stromatolite precipitation and the beginning of the deposition of thinly laminated limestone, where the latter lithotype shows positive $\delta^{13}\text{C}$ values. A more stable lake-water thermal stratification (meromixis) relates

to this trend. In this context, the aqueous HCO_3^- of the epilimnion waters tends to be more balanced in relation to atmospheric CO_2 . A prolongation of the chemical stratification of lake waters would then result in an enrichment of the $\delta^{13}\text{C}$ values of the DIC pool, with limited input of ^{12}C -rich waters to the epilimnion (Cohen 2003; Heimhofer et al. 2010). This behavior indicates that distinct CaCO_3 precipitation mechanisms dictate the genesis of the two carbonate lithotypes, where the microcrystals, which compose most of the thinly laminated limestones, were formed in the pelagic zones and then settled to the lake bottom.

The positive correlation between Mn and Ca also points to the formation of Mn(II) carbonate minerals (e.g., rhodochrosite, kutnahorite), with little or no precipitation as sulfide minerals, following the model proposed by Herndon et al. (2018). Part of the calcite precipitated in the epilimnion dissolves as it settles into the chemocline, where Mn-carbonate nucleates, with no reductive dissolution of Mn(IV) oxides. Notwithstanding, more comprehensive studies about which parameters would control the precipitation of Mn in the water column and its incorporation into the sediments of the Crato Member's paleolake are needed.

A simplified three-step depositional model comprising each lithotype in the studied interval and its respective paleoenvironmental settings are illustrated in Figure 12. It starts with: I) the deposition of the organic shales, which occurred in the benthic and anoxic zones of the paleolake, with a significant contribution of organic matter sourced presumably by a combination of autochthonous and allochthonous material. Also, there was the distinctive incorporation of ostracod valves throughout the deposition of this lithotype. II) Biologically induced mineralization (organomineralization) took place as the forming process of the nodular limestones (planar stromatolites), occurring in the anoxic littoral to sublittoral settings of a very calm and closed lake, which allowed the lateral continuity of laminae preservation. Low water and sediment inflow rates prevailed at this time, favoring carbonate concentration and precipitation. III) Finally, precipitation controlled by seasonal variations occurred in the pelagic and more oxygenated zones (epilimnion) of a chemically stratified lake. The formed microcrystals then settled in the anoxic benthic zone (hypolimnion). Low inflow rates of water and sediment also contributed to prevent water mixing and helped maintain stratification.

The remarkable similarity observed between the stromatolites of the studied interval and its extensive lateral occurrence testify to the formation of a kilometer-wide biostrome, which reflects the onset of biochemical changes over large distances and is necessarily a result of a regional event (Ibarra and Corsetti 2016). The described geochemical data suggest that this phenomenon occurred in a closed to semi-closed continuously stratified paleolake (Leng and Marshall 2004; Xiong et al. 2021).

Microbialite spreading as responsive to major geologic events is frequently reported in the literature, because dramatic environmental changes and geochemistry can affect water saturation, oxygenation, and reduction of EPS interaction (competition, grazing) with diverse eukaryotic organisms. This trend is observed in relatively recent and locally relevant climatic changes (e.g., Villafañe et al. 2021), in global-scale events, like the one which signal the Permian–Triassic boundary (e.g., Kershaw et al. 2002; Hips and Haas 2006), and was also documented in environmentally stressful events related to the early Aptian (Immenhauser et al. 2005), among others (see Mata and Bottjer 2012).

Nevertheless, Aptian microbialite occurrences in neighboring basins, like the ones of the Codó Formation of Parnaíba Basin (Bahniuk et al. 2015) and the Crato Formation of Jatobá Basin (Gratzer et al. 2013), exhibit similar characteristics (although not the same lamination pattern) and may be related to processes like those that formed the stromatolites described herein, possibly deriving from the same event.

It is challenging to identify the precise factors contributing to the formation of this vast biostrome and its possible microbial occurrences. However, the onset of abrupt rises in atmospheric CO_2 levels during Oceanic Anoxic Events (OAEs) could have induced climatic disturbances and subsequent environmental changes that impacted the growth and

propagation of stromatolite ecosystems, as suggested by Pietzsch et al. (2020) for the coeval Barra Velha Formation.

CONCLUSIONS

- 1) Through a multiscale analysis of well cores, we characterize distant but nearly identical occurrences of relatively thin layers of sedimentary rocks. This approach reveals the extensive occurrence of a succession encompassing three lithotypes and their main characteristics. Geochemical investigation allows us to reconstruct the main attributes of the depositional paleoenvironment of these lithotypes. The sedimentation of the succession occurred in anoxic conditions of the benthic zone of the sub-marginal area of a closed to semi-closed paleolake.
- 2) The stromatolites of the studied horizon show well-demarcated internal fabrics and compositional variations, which reflect changes in environmental settings on regional and local scales. The record of similar fabric-pattern occurrences in distant locations suggests that the processes controlling these changes must have been relatively uniform, and thus reflect regional processes. However, overall differences in chemical composition of the samples are notable and interpretable as an expression of local environmental and diagenetic settings.
- 3) The stromatolite bodies were formed chiefly by *in situ* precipitation triggered by organic-matter degradation performed by bacteria (presumably SRB). This process occurred in the sublittoral benthic zone of a freshwater lake and under anoxic, possibly euxinic, conditions. The precipitation of the thinly laminated limestones that overlie the stromatolites marks an apparent stage of water stratification, where calcite microcrystals formed in the epilimnion and were deposited on the lake bottom.
- 4) The precipitation of a kilometer-wide biostrome, traceable in an area of about 600 km², is evidence of a regional geological event. This microbialitic horizon lies among the first-deposited limestones of the Crato Member and is assigned as a new marker bed in the Araripe Basin. Furthermore, the horizon described here is one of the world's best examples of an ancient microbialite field, with unparalleled similarity and traceability between exposures.

ACKNOWLEDGMENTS

The authors gratefully acknowledge the research and development project “Correlação estratigráfica, evolução paleoambiental e paleogeográfica e perspectivas exploratórias do Andar Alagoas,” sponsored by Shell Brasil Petróleo Ltda. with resources allocated to R&D institutions accredited by the Brazilian National Petroleum, Natural Gas and Biofuels Agency (technical cooperation agreement #20219-2). We thank editor Dr. John Southard, associate editor James Bishop, and an anonymous reviewer for their comments and suggestions on the manuscript.

REFERENCES

- ARAI, M., 1999, A transgressão marinha mesocretácea: sua implicação no paradigma na reconstituição paleogeográfica do Cretáceo no Brasil: V Simpósio Sobre o Cretáceo do Brasil, Boletim, p. 577–582.
- ARAÚJO, B.C., GAMA, F., ALMEIDA, F.N., Jr., NASCIMENTO, T., SILVEIRA, L.F., DUARTE, G., BORCHI, L., BRAGA, M.A.S., AND FIGUEIREDO, J.P., 2019, Refining structural interpretation by using the composite map of the vertical derivatives of aeromagnetic anomaly data: Rio de Janeiro, 16th International Congress of the Brazilian Geophysical Society, Proceedings.
- ARENAS, C., CASANOVA, J., AND PARDO, G., 1997, Stable-isotope characterization of the Miocene lacustrine systems of Los Monegros (Ebro Basin, Spain): palaeogeographic and palaeoclimatic implications: Palaeogeography, Palaeoclimatology, Palaeoecology, v. 128, p. 133–155.
- ARMENTEROS, I., 2010, Diagenesis of carbonates in continental settings, in Alonso-Zarza, A.M., and Tanner, L.H., eds., Carbonates in Continental Settings: Geochemistry, Diagenesis and Applications: Elsevier, Developments in Sedimentology 62, p. 61–151.
- ARR, G., REIMER, A., AND REITNER, J., 2003, Microbialite formation in seawater of increased alkalinity, Satonda Crater Lake, Indonesia: Journal of Sedimentary Research, v. 73, p. 105–127.

- ASSINE, M.L., 2007, Bacia do Araripe: Boletim de Geociências da Petrobras, v. 15, p. 371–389.
- BADDOUH, M., CARROLL, A.R., MEYERS, S.R., BEARD, B.L., AND JOHNSON, C.M., 2017, Chronostratigraphic correlation of lacustrine deposits using $^{87}\text{Sr}/^{86}\text{Sr}$ ratios, Eocene Green River Formation, Wyoming, U.S.A.: Journal of Sedimentary Research, v. 87, p. 406–423.
- BÁEZ, A.M., MOURA, G.J.B., AND GÓMEZ, R.O., 2009, Anurans from the Lower Cretaceous Crato Formation of northeastern Brazil: implications for the early divergence of neobatrachians: Cretaceous Research, v. 30, p. 829–846.
- BAHNIUK, A.M., ANJOS, S., FRANÇA, A.B., MATSUDA, N., EILER, J., MCKENZIE, J.A., AND VASCONCELOS, C., 2015, Development of microbial carbonates in the Lower Cretaceous Codó Formation (north-east Brazil): implications for interpretation of microbialite facies associations and palaeoenvironmental conditions: Sedimentology, v. 62, p. 155–181.
- BARLING, N., MARTILL, D.M., AND HEADS, S.W., GALLIEN, F., 2015, High fidelity preservation of fossil insects from the Crato Formation (Lower Cretaceous) of Brazil: Cretaceous Research, v. 52, p. 605–622.
- BARLING, N., MARTILL, D.M., AND HEADS, S.W., 2020, A geochemical model for the preservation of insects in the Crato Formation (Lower Cretaceous) of Brazil: Cretaceous Research, v. 116, no. 104608.
- BATES, R.L., AND JACKSON, J.A., 1980, Glossary of Geology: American Geological Institute, 751 p.
- BERNER, R.A., 1985, Sulphate reduction, organic matter decomposition and pyrite formation: Royal Society of London, Philosophical Transactions, Series A, Mathematical and Physical Sciences, v. 315, p. 25–38.
- BEURLEN, K., 1962, A Geologia da Chapada do Araripe: Academia Brasileira de Ciências, Anais, v. 34, p. 365–370.
- BOBCO, F.E.R., GOLDBERG, K., AND BARDOLA, T.P., 2017, Modelo deposicional do Membro Ipubi (Bacia do Araripe, nordeste do Brasil) a partir da caracterização faciológica, petrográfica e isotópica dos evaporitos: Pesquisa em Geociências, v. 44, p. 431–451.
- BOHACS, K.M., CARROLL, A.R., NEAL, J.E., AND MANKIEWICZ, P.J., 2000, Lake-basin type, source potential, and hydrocarbon character: an integrated-sequence-stratigraphic-geochemical framework, in Gierlowski-Kordesch, E.H., and Kelts, K.R., eds., Lake Basins through Space and Time: American Association of Petroleum Geologists, Studies in Geology 46, p. 3–34.
- BOYLE, J., 2001, Redox remobilization and the heavy metal record in lake sediments: a modelling approach: Journal of Paleolimnology, v. 26, p. 423–431.
- BRITO-NEVES, B.B., 1990, A Bacia do Araripe no contexto geotectônico regional: Crato, Brazil, I Simpósio Bacia do Araripe e Bacias Interiores do Nordeste, Atas, p. 21–33.
- BUNEVICH, R.B., BORGHI, L., GABAGLIA, G.P.R., TERRA, G.J.S., FREIRE, E.B., LYKAWKA, R., AND FRAGOSO, D.G.C., 2017, Microbialites da Sequência Balbuena IV (Damião), Bacia de Salta, Argentina: caracterização de intrabioarquitecturas e de microciclos: Pesquisas em Geociências, v. 44, p. 177–202.
- BUSTILLO, M.A., 2010, Silicification of continental carbonates, in Alonso-Zarza, A.M., and Tanner, L.H., eds., Carbonates in Continental Settings: Geochemistry, Diagenesis and Applications: Elsevier, Developments in Sedimentology 62, p. 153–178.
- CALVO, J.P., RODRIGUEZ-PASCUA, M., MARTIN-VELAZQUEZ, S., JIMENEZ, S., AND DE VICENTE, G., 1998, Microdeformation of lacustrine laminite sequences from Late Miocene formations of SE Spain: an interpretation of loop bedding: Sedimentology, v. 45, p. 279–292.
- CAMACHO, C.R., AND SOUSA, F.R.F.R.O., 2017, O arcabouço estrutural da Bacia Sedimentar do Araripe, Província Borborema, baseado em dados aeromagnetométricos: Geologia USP, Série Científica, v. 17, p. 149–161.
- CAMPBELL, C.V., 1967, Lamina, lamina set, bed and bedset: Sedimentology, v. 8, p. 7–36.
- CARROLL, A.R., AND BOHACS, K.M., 1999, Stratigraphic classification of ancient lakes: balancing tectonic and climatic controls: Geology, v. 27, p. 99–102.
- CARVALHO, I.S., AND VIANA, M.S.S., 1993, Os Conchostráceos da Bacia do Araripe: Academia Brasileira de Ciências, Anais, v. 65, p. 181–188.
- CARVALHO, I.S., AGNOLINI, F., ROLANDO, M.A.A., NOVAS, F.E., XAVIER-NETO, J., FREITAS, F.I., AND ANDRADE, J.A.F.G., 2019, A new genus of pipimorph frog (Anura) from the Early Cretaceous Crato Formation (Aptian) and the evolution of South American tongueless frogs: Journal of South American Earth-Sciences, v. 92, p. 222–233.
- CASANOVA, J., AND HILLAIRE-MARCEL, C., 1993, Carbon and oxygen isotopes in African lacustrine stromatolites: palaeohydrological interpretation, in Swart, P.K., Lohmann, K. C., Mckenzie, J., and Savin, S., eds., Climate Change in Continental Isotopic Records: v. 78, p. 123–133.
- CATTO, B., JANHERT, R.J., WARREN, L.V., VAREJÃO, F.G., AND ASSINE, M.L., 2016, The microbial nature of laminated limestones: lessons from the Upper Aptian, Araripe Basin, Brazil: Sedimentary Geology, v. 341, p. 304–315.
- CAYEUX, L., 1935, Les Roches Sédimentaires de France: Roches Carbonatées (Calcaires et Dolomies): Paris, 463 p.
- CHAGAS, D.B., ASSINE, M.L., AND FREITAS, F.I., 2007, Fácies sedimentares e ambientes deposicionais da Formação Barbalha no Vale do Cariri, Bacia do Araripe, Nordeste do Brasil: Geociências, v. 26, p. 313–322.
- CHOUHDURI, A., SARKAR, S., ALTERMANN, W., MUKHOPADHYAY, S., AND BOSE, P.K., 2016, Lakshanhatti stromatolite, India: biogenic or abiogenic?: Journal of Palaeogeography, v. 5, p. 292–310.
- COBBOLD, P.R., ZANELLA, A., RODRIGUES, N., AND LOSETH, H., 2013, Bedding-parallel fibrous veins (beef and cone-in-cone): worldwide occurrence and possible significance in terms of fluid overpressure, hydrocarbon generation and mineralization: Marine and Petroleum Geology, v. 43, p. 1–20.
- COHEN, A.S., 2003, Paleolimnology: The History and Evolution of Lake Systems: Oxford University Press, 500 p.
- COHEN, A.S., TALBOT, M.R., AWRAMIK, S.M., DETTMAN, D.L., AND ABELL, P., 1997, Lake level and paleoenvironmental history of Lake Tanganyika, Africa, as inferred from late Holocene and modern stromatolites: Geological Society of America, Bulletin, v. 109, p. 444–460.
- CORELLA, J.P., BRAUER, A., MANGILI, C., RULL, V., VEGAS-VILARRUBIA, T., MORELLÓN, M., AND VALERO-GARCÉS, B.L., 2012, The 1.5-ka varved record of Lake Montcortés (southern Pyrenees, NE Spain): Quaternary Research, v. 78, p. 323–332.
- CUSTÓDIO, M.A., QUAGLIO, F., WARREN, L.V., SIMÕES, M.G., FÜRSICH, F.T., PERINOTTO, J.A.J., AND ASSINE, M.L., 2017, The transgressive-regressive cycle of the Romualdo Formation (Araripe Basin): sedimentary archive of the Early Cretaceous marine incursion in the interior of Northeast Brazil: Sedimentary Geology, v. 359, p. 1–15.
- DAVIES, S.J., LAMB, H.F., AND ROBERTS, S.J., 2015, Micro-XRF Core scanning in paleolimnology: recent developments, in Croudace, I.W., and Rothwell, R.G., eds., Micro-XRF Studies of Sediment Cores: Applications of a Non-Destructive Tool for the Environmental Sciences: Springer, Developments in Paleoenvironmental Research 117, p. 189–226.
- DAVISON, W., 1993, Iron and manganese in lakes: Earth-Science Reviews, v. 34, p. 119–163.
- DE BOEVER, E., BRASIER, A.T., FOUBERT, A., AND KELE, S., 2017, What do we really know about early diagenesis of non-marine carbonates?: Sedimentary Geology, v. 361, p. 25–51.
- DE MOTT, L.M., NAPIERALSKI, S.A., JUNIUM, C.K., TEECE, M., AND SCHOLZ, C.A., 2020, Microbially influenced lacustrine carbonates: a comparison of Late Quaternary Lahontan tufa and modern thrombolite from Fayetteville Green Lake, NY: Geobiology, v. 18, p. 93–112.
- DEOCAMPO, D.M., 2010, The geochemistry of continental carbonates, in Alonso-Zarza, A.M., and Tanner, L.H., eds., Carbonates in Continental Settings: Geochemistry, Diagenesis and Applications: Elsevier, Developments in Sedimentology 62, p. 1–59.
- DES MARAIS, D.J., 1995, The biogeochemistry of hypersaline microbial mats, in Jones, J. G., ed., Advances in Microbial Ecology: v. 14, p. 251–274.
- DOEBBERT, A., JOHNSON, C.M., CARROLL, A.R., BEARD, B.L., PIETRAS, J.T., CARSON, M.R., NORSTED, B., AND THROCKMORTON, L.A., 2014, Controls on Sr isotopic evolution in lacustrine systems: Eocene Green River Formation, Wyoming: Chemical Geology, v. 380, p. 172–189.
- DIAS, J.J., AND CARVALHO, I.S., 2020, Remarkable fossil crickets preservation from Crato Formation (Aptian, Araripe Basin), a Lagerstätten from Brazil: Journal of South American Earth Sciences, v. 98, no. 102443.
- DUARTE, G., AND BORGHI, L., 2018, Petrografia das fácies evaporíticas sulfatadas do Membro Ipubi, Formação Santana (Bacia do Araripe): Instituto de Geociências, Anuário v. 41, p. 606–613.
- DUPRAZ, C., AND VISSCHER, P.T., 2005, Microbial lithification in marine stromatolites and hypersaline mats: Trends in Microbiology, v. 13, p. 429–438.
- DUPRAZ, C., VISSCHER, P.T., BAUMGARTNER, L.K., AND REID, R.P., 2004, Microbe–mineral interactions: early carbonate precipitation in a hypersaline lake (Eleuthera Island, Bahamas): Sedimentology, v. 51, p. 745–765.
- DUPRAZ, C., REID, R.P., BRAISSANT, O., DECHO, A.W., NORMAN, R.S., AND VISSCHER, P.T., 2009, Processes of carbonate precipitation in modern microbial mats: Earth-Science Reviews, v. 96, p. 141–162.
- DUVERGER, A., BERG, J.S., BUSIGNY, V., GUYOT, F., BERNARD, S., AND MILOT, J., 2020, Mechanisms of pyrite formation promoted by sulfate-reducing bacteria in pure culture: Frontiers in Earth Science, v. 8, no. 588310.
- EL HAJI, L., HORNE, D.J., BAUDIN, F., GÈZE, R., AND AZAR, D., 2021, The first non-marine ostracod fauna from the Lower Barremian dysodiles of Lebanon: Lethaia, v. 54, p. 127–159.
- EVANS, G., AUGUSTINUS, P., GADD, P., ZAWADZKI, A., AND DITCHFIELD, A., 2019, A multi-proxy m-XRF inferred lake sediment record of environmental change spanning the last ca. 2230 years from Lake Kanono, Northland, New Zealand: Quaternary Science Reviews, v. 225, no. 106000.
- FAMBRINI, G.L., MENEZES-FILHO, J.A.B., JESUINO, P.C.L., SILVESTRE, D.C., LEMOS, D.R., AND NEUMANN, V.H.L., 2016, Caracterização dos sistemas deposicionais da Formação Barbalha, Bacia do Araripe, Nordeste do Brasil: Comunicações Geológicas, v. 103, p. 51–65.
- FARMER, J.D., 1992, Grazing and bioturbation in modern microbial mats, in Schopf, W., and Klein, C., eds., The Proterozoic Biosphere: A Multidisciplinary Study: Cambridge University Press, p. 295–297.
- FIGUEIREDO, R.G., AND KELLNER, A.W.A., 2009, A new crocodylomorph specimen from the Araripe Basin (Crato Member, Santana Formation), northeastern Brazil: Paläontologische Zeitschrift, v. 83, p. 323–331.
- FLÜGEL, E., 2010, Microfacies of Carbonate Rocks, Second Edition: Springer, 984 p.
- GIERLOWSKI-KORDESCH, E.H., 2010, Lacustrine carbonates, in Alonso-Zarza, A.M., and Tanner, L.H., eds., Carbonates in Continental Settings: Facies, Environments and Processes: Developments in Sedimentology: Elsevier 61, p. 1–101.
- GLUNK, C., DUPRAZ, C., BRAISSANT, O., GALLAGHER, K.L., VERRECHIA, E.P., AND VISSCHER, P.T., 2011, Microbially mediated carbonate precipitation in a hypersaline lake, Big Pond (Eleuthera, Bahamas): Sedimentology, v. 58, p. 720–738.
- GRATZER, R., NEUMANN, H., VORTSCH, W., ROCHA, D.E.A., AND BETCHEL, A., 2013, Stable isotopes of organics and inorganics, clay mineralogy and chemical environment of an Aptian lacustrine succession in northeastern Brazil, in Bojar, A.-V., Melinte-Dobrinescu,

- M.C., and Smit, J., eds., *Isotopic Studies in Cretaceous Research: Geological Society of London, Special Publication 382*, p. 157–182.
- Grimaldi, D.A., ed., 1990, *Insects from the Santana Formation, Lower Cretaceous of Brazil: American Museum of Natural History, Bulletin*, v. 195, 191 p.
- HASHIMOTO, A.T., APPI, C.J., SOLDAN, A.L., AND CERQUEIRA, J.R., 1987, O Neo-Alagoas nas bacias do Ceará, Araripe e Potiguar (Brasil): caracterização estratigráfica e paleoambiental: *Revista Brasileira de Geociências*, v. 17, p. 118–122.
- HEIMHOFER, U., ARIZTEGUI, D., LENNIGER, M., HESSELBO, S.P., MARTILL, D.M., AND RIOS-NETTO, A.M., 2010, Deciphering the depositional environment of the laminated Crato fossil beds (Early Cretaceous, Araripe Basin, North-eastern Brazil): *Sedimentology*, v. 57, p. 677–694.
- HERNDON, E.M., HAVIG, J.R., SINGER, D.M., MCCORMICK, M.L., AND KUMR L.R., 2018, Manganese and iron geochemistry in sediments underlying the redox-stratified Fayetteville Green Lake: *Geochimica et Cosmochimica Acta*, v. 231, p. 50–63.
- HILLAIRE-MARCEL, C., AND CASANOVA, J., 1987, Isotopic hydrology and paleohydrology of the Magadi (Kenya)-Natron (Tanzania) Basin during the Late Quaternary: *Paleogeography, Paleoclimatology, Paleoecology*, v. 58, p. 155–181.
- HIPS, K., AND HAAS, J., 2006, Calcimicrobial stromatolites at the Permian–Triassic boundary in a western, Tethyan section, Bükk Mountains, Hungary: *Sedimentary Geology*, v. 185, p. 239–253.
- HUNTER, J.D., 2007, *Matplotlib: a 2-D graphics environment: Computing in Science & Engineering*, v. 9, p. 90–95.
- IBARRA, Y., AND CORSETTI, F.A., 2016, Lateral comparative investigation of stromatolites: astrobiological implications and assessment of scales of control: *Astrobiology*, v. 16, p. 1–11.
- IMMENHAUSER, A., HILLGÄRTNER, H., AND VAN BENTUM, E., 2005, Microbial–foraminiferal episodes in the Early Aptian of the southern Tethyan margin: ecological significance and possible relation to oceanic anoxic event 1a: *Sedimentology*, v. 52, p. 77–99.
- INESTO, M., GUTIÉRREZ-SILVA, P., DIAS, J., CARVALHO, I.S., BUSCALIONI, A.D., AND LÓPEZ-ARCHILLA, A.I., 2021, Soft tissue histology of insect larvae decayed in laboratory experiments using microbial mats: taphonomic comparison with Cretaceous fossil insects from the exceptionally preserved biota of Araripe, Brazil: *Paleogeography, Palaeoclimatology, Paleoecology*, v. 564, no. 110156.
- JANHERT, R.J., AND COLLINS, L.B., 2013, Controls on microbial activity and tidal flat evolution in Shark Bay, Western Australia: *Sedimentology*, v. 60, p. 1071–1099.
- KALKOWSKY, E., 1908, Oolith und Stromatolith im norddeutschen Buntsandstein: *Deutschen Geologischen Gesellschaft, Zeitschrift*, v. 60, p. 68–125.
- KELTS, K., 1988, Environments of deposition of lacustrine petroleum source rocks: an introduction, in Fleet, A.J., Kelts, K., and Talbot, M.R., eds., *Lacustrine Petroleum Source Rocks: Geological Society of London, Special Publication 40*, p. 3–26.
- KELTS, K., AND HSÜ, K.J., 1978, Freshwater carbonate sedimentation, in Lerman, A., ed., *Lakes: Chemistry, Geology, Physics: Springer-Verlag*, p. 295–324.
- KELTS, K., AND TALBOT, M., 1990, Lacustrine carbonates as geochemical archives of environmental change and biotic–abiotic interactions, in Tilzer, M.M., and Serruya, C., eds., *Large Lakes: Ecological Structure and Function: Springer-Verlag*, p. 288–315.
- KERSHAW, S., GUO, L., SWIFT, A., AND FAN, J., 2002, Microbialites in the Permian–Triassic boundary interval in central China: structure, age and distribution: *Facies*, v. 47, p. 83–89.
- KRÖTH, M., BORGHI, L., BOBCO, F.E.R., ARAÚJO, B.C., SILVEIRA, L.F., DUARTE, G., FERREIRA, L. O., GUERRA-SOMMER, M., AND MENDONÇA, J.O., 2021, Aptian shell beds from the Romualdo Formation (Araripe Basin): implications for paleoenvironment and paleogeographical reconstruction of the Northeast of Brazil: *Sedimentary Geology*, v. 426, no. 106025.
- KYLANDER, M.E., AMPEL, L., WOHLFARTH, B., AND VERES, D., 2011, High-resolution X-ray fluorescence core scanning analysis of Les Echets (France) sedimentary sequence: new insights from chemical proxies: *Journal of Quaternary Science*, v. 26, p. 109–117.
- LAMB, H.F., LENG, M.J., TELFORD, R.J., AYENEW, T., AND UMER, M., 2007, Oxygen and carbon isotope composition of authigenic carbonate from an Ethiopian lake: a climate record of the last 2000 years: *The Holocene*, v. 17, p. 517–526.
- LENG, M.J., AND MARSHALL, J.D., 2004, Palaeoclimate interpretation of stable isotope data from lake sediment archives: *Quaternary Science Reviews*, v. 23, p. 811–831.
- LETTERÓN, A., FOURNIER, F., HAMON, Y., VILLIER, L., MARGEREL, J.-P., BOUCHE, A., FEIST, M. AND JOSEPH, P., 2017, Multi-proxy paleoenvironmental reconstruction of saline lake carbonates: paleoclimatic and paleogeographic implications (Priabonian–Rupelian, Issirac Basin, SE France): *Sedimentary Geology*, v. 358, p. 97–120.
- MABESONE, J.M., AND TINOCO, I.M., 1973, Paleocology of the Aptian Santana Formation (Northeastern Brazil): *Paleogeography, Palaeoclimatology, Paleoecology*, v. 14, p. 97–118.
- MACKERETH, F.J.H., 1966, Some chemical observations on post-glacial lake sediments: *Royal Society of London, Philosophical Transactions, Series B, Biological Sciences*, v. 765, p. 165–213.
- MAISANO, L., QUIJADA, I.E., CUADRADO, D.G., PERILLO, V.L., PAN, J., AND MARTINEZ, A.M., 2020, Carbonate laminae recorded in a siliciclastic tidal flat colonized by microbial mats: *Sedimentary Geology*, v. 405, no. 105702.
- MAKARKIN, V.N., AND MENON, F., 2005, New species of the Mesochrysoptidae (Insecta, Neuroptera) from the Crato Formation of Brazil (Lower Cretaceous), with taxonomic treatment of the family: *Cretaceous Research*, v. 26, p. 801–812.
- MARTILL, D.M., 2007, The geology of the Crato Formation, in Martill, D.M., Bechly, G., and Loveridge, R.F., eds., *The Crato Fossil Beds of Brazil: Window into an Ancient World: Cambridge University Press*, p. 8–24.
- MARTILL, D.M., BECHLY, G., AND LOVERIDGE, R.F., 2007a, The Crato Fossil Beds of Brazil: Window into an Ancient World. Cambridge University Press, 625 p.
- MARTILL, D.M., LOVERIDGE, R., AND HEIMHOFER, U., 2007b, Halite pseudomorphs in the Crato Formation (Early Cretaceous, Late Aptian–Early Albian), Araripe Basin, northeast Brazil: further evidence for hypersalinity: *Cretaceous Research*, v. 28, 613–620.
- MARTILL, D.M., BRITO, P.M., AND DONOVAN, S.K., 2021, There are rudists in Brazil! Derived examples of cf. *Amphitriscoelus* Harris and Hodson, 1922, in the Araripe Basin, north-east Brazil: implications for dating of the fossil Lagerstätten of the Santana and Crato formations: *Cretaceous Research*, v. 120, 104718.
- MARTÍN-BELLO, L., ARENAS, C., AND JONES, B., 2019, Lacustrine stromatolites: useful structures for environmental interpretation: an example from the Miocene Ebro Basin: *Sedimentology*, v. 66, p. 2098–2133.
- MATA, S.A., AND BOTTIER, D.J., 2012, Microbes and mass extinctions: paleoenvironmental distribution of microbialites during times of biotic crisis: *Geobiology*, v. 10, p. 3–24.
- MATOS, R.M.D., 1992, The northeast Brazilian rift system: Tectonics, v. 11, p. 766–791.
- MATOS, R.M.D., 2000, Tectonic evolution of the equatorial South Atlantic: American Geophysical Union, *Geophysical Monograph*, v. 115, p. 331–354.
- MIRANDA, T.S., MAGALHÃES, J.R.G., BARBOSA, J.A., CORREIA FILHO, O., AND ALENCAR, M.L., 2014, Araripe Basin, NE Brazil: a rift basin implanted over a previous pull-apart system?: 4th Atlantic Conjugate Margins Conference, Proceedings.
- MOHR, B.A.R., AND EKLUND, H., 2003, *Araripia florifera*, a magnoliid angiosperm from the Lower Cretaceous Crato Formation (Brazil): Review of Palaeobotany and Palynology, v. 126, p. 279–292.
- Munsell Color, 2009, *Geological Rock-Color Chart: with genuine Munsell® color chips: Munsell Color, X-Rite*.
- NEUMANN, V.H., 1999, *Estratigrafia, Sedimentología, Geoquímica y Diagénesis de los sistemas lacustres Aptiense–Albienses de la Cuenca de Araripe (NE Brasil) [Ph.D. Thesis]: Universitat de Barcelona*, 250 p.
- NEUMANN, V.H., BORREGO, A.G., CABRERA, L., AND DINO, R., 2003, Organic matter composition and distribution through the Aptian–Albian lacustrine sequences of the Araripe Basin, northeastern Brazil: *International Journal of Coal Geology*, v. 54, p. 21–40.
- OLIVERI, E., NERI, R., BELLANCA, A., AND RIDING, R., 2010, Carbonate stromatolites from a Messinian hypersaline setting in the Caltanissetta Basin, Sicily: petrographic evidence of microbial activity and related stable isotope and rare earth element signatures: *Sedimentology*, v. 57, p. 142–161.
- Olympus VANTA, VMW RoHS LODs (P/N: 806-439-EN Rev.A).
- OSCHMANN, W., 2000, Microbes and black shales, in Riding, R., and Awramik, S.M., eds., *Microbial Sediments: Springer*, p. 137–148.
- OSÉS, G.L., PETRI, S., BECKER-KERBER, B., ROMERO, G.R., RIZZUTTO, M.A., RODRIGUES, F., GALANTE, D., SILVA, T.F., CURADO, J.F., RANGEL, E.C., RIBEIRO, R.P., AND PACHECO, M.L.A. F., 2016, Deciphering the preservation of fossil insects: a case study from the Crato Member, Early Cretaceous of Brazil: *PeerJ*, v. 4, no. e2756.
- PERRI, E., AND SPADAFORA, A., 2011, Evidence of microbial biomineralization in modern and ancient stromatolites, in Tewari, V., and Seckbach, J., eds., *Stromatolites: Interaction of Microbes with Sediments: Springer, Cellular Origin, Life in Extreme Habitats and Astrobiology*, v. 18, p. 631–649.
- PERRI, E., TUCKER, M., AND SPADAFORA, A., 2012, Carbonate organo-mineral micro- and ultrastructures in sub-fossil stromatolites: Marion Lake, South Australia: *Geobiology*, v. 10, p. 105–117.
- PIETZSCH, R., TEDESCHI, L.R., OLIVEIRA, D.M., DOS ANJOS, C.W.D., VAZQUEZ, J.C., AND FIGUEIREDO, M.F., 2020, Environmental conditions of deposition of the Lower Cretaceous lacustrine carbonates of the Barra Velha Formation, Santos Basin (Brazil), based on stable carbon and oxygen isotopes: a continental record of pCO₂ during the onset of the Oceanic Anoxic Event 1a (OAE 1a) interval?: *Chemical Geology*, v. 535, no. 119457.
- PLATT, N.H., AND WRIGHT, V.P., 1991, Lacustrine carbonates: facies models, facies distributions and hydrocarbon aspects, in Anádon, P., Cabrera, L., and Kelts, K., eds., *Lacustrine Facies Analysis: International Association of Sedimentologists, Special Publication 13*, p. 57–74.
- PONTE, F.C., AND APPI, C.J., 1990, Proposta de revisão da coluna litoestratigráfica da Bacia do Araripe: *Congresso Brasileiro de Geologia 36, Anais*, v. 1, p. 211–226.
- PONTE, F.C., AND PONTE FILHO, F.C., 1996, *Estrutura geológica e evolução tectônica da Bacia do Araripe: Departamento Nacional de Pesquisa Mineral, Internal Report*, 68 p.
- QUYE-SAWYER, J., VANDENGINSTE, V., AND JOHNSTON, K.J., 2015, Application of handheld energy-dispersive X-ray fluorescence spectrometry to carbonate studies: opportunities and challenges: *Journal of Analytical Atomic Spectrometry*, v. 30, p. 1490–1499.
- RENAUT, R.W., AND GIERLOWSKI-KORDESCH, E.H., 2010, *Lakes*, in James, N.P., and Dalrymple, R.W., eds., *Facies Models 4: The Geological Association of Canada, GEOText 6*, p. 541–576.
- RENAUT, R.W., JONES, B., AND TIERCELIN, J.J., 1998, Rapid *in situ* silicification of microbes at Loburu hot springs, Lake Bogoria, Kenya Rift Valley: *Sedimentology*, v. 45, p. 1083–1103.
- REGALI, M.S.P., 2001, *Palinoestratigrafia dos sedimentos cretácicos da bacia do Araripe e das bacias interiores do Nordeste, Brasil: Atas, Simpósio sobre a Bacia do Araripe e Bacias Interiores do Nordeste*, p. 101–108.
- RIBEIRO, A.C., RIBEIRO, G.C., VAREJÃO, F.G., BATTIROLA, L.D., PESSOA, E.M., SIMÕES, M.G., WARREN, L.V., RICCOMINI, C., AND POYATO-ARIZA, F.J., 2021, Towards an actualistic view of the Crato Konservat–Lagerstätte paleoenvironment: a new hypothesis as an Early Cretaceous (Aptian) equatorial and semi-arid wetland: *Earth-Science Reviews*, v. 216, no. 103573.
- RIDING, R., 1999, The term stromatolite: towards an essential definition: *Lethaia*, v. 32, p. 321–330.

- RIDING, R., 2000, Microbial carbonates: the geological record of calcified bacterial–algal mats and biofilms: *Sedimentology*, v. 47, Suppl. 1, p. 179–214.
- RIDING, R., AND TOMÁS, S., 2006, Stromatolite reef crusts, Early Cretaceous, Spain: bacterial origin of in situ-precipitated peloid microspar?: *Sedimentology*, v. 53, p. 23–34.
- RIOS-NETTO, A.M., PAULA-FREITAS, A.B.L., CARVALHO, I.S., REGALI, M.S.P., BORGHI, L., AND FRANCISCO, I.F., 2012, Formalização estratigráfica do Membro Fundão, Formação Rio da Bateira, Cretáceo Inferior da Bacia do Araripe, Nordeste do Brasil: *Revista Brasileira de Geociências*, v. 42, p. 281–292.
- RODRIGUES, K.C., 2015, Caracterização petrográfica dos “carbonatos” laminados do Membro Crato, Bacia do Araripe, Nordeste do Brasil [BS Thesis]: Universidade Federal do Rio Grande do Sul, 167 p.
- SANTOS, M.E.C.M., 1982, Ambiente deposicional da Formação Santana–Chapada do Araripe (PE/PI/CE): Congresso Brasileiro de Geologia 32, Anais, p. 1413–1426.
- SCHIED, C., MUNIS, M.B., AND PAULINO, J., 1978, Projeto Santana, Relatório final da Etapa II: CPRM, <http://rigeo.cprm.gov.br/jspui/handle/doc/7690>.
- SCHILDOWSKI, M., 2000, Carbon isotopes and microbial sediments, in Riding, R.E., and Awramik, S.M., eds., *Microbial Sediments*: Springer, p. 84–95.
- SHAPIRO, R.S., 2000, A comment on the systematic confusion of thrombolites: *Palaios*, v. 15, p. 166–169.
- SILVA, M.A.M., 1983, The Araripe Basin, northeastern Brazil: regional geology and facies analysis of a Lower Cretaceous evaporitic depositional complex [Ph.D. Thesis]: Columbia University, 290 p.
- SILVA, M.A.M., 1988, Evaporitos do Cretáceo da Bacia do Araripe: ambientes de deposição e história diagenética: *Boletim de Geociências da Petrobras*, v. 2, p. 53–63.
- SUAREZ-GONZALEZ, P., QUIJADA, I.E., BENITO, M.I., MAS, R., MERINERO, R., AND RIDING, R., 2014, Origin and significance of lamination in Lower Cretaceous stromatolites and proposal for a quantitative approach: *Sedimentary Geology*, v. 300, p. 11–27.
- TALBOT, M.R., 1990, A review of paleohydrological interpretation of carbon and oxygen isotopic ratios in primary lacustrine carbonates: *Chemical Geology, Isotope Geoscience Section*, v. 80, p. 261–279.
- TALBOT, M.R., AND KELTS, K., 1986, Primary and diagenetic carbonates in the anoxic sediments of Lake Bosumtwi, Ghana: *Geology*, v. 14, p. 912–916.
- TAYLOR, K.G., AND MACQUAKER, J.H.S., 2000, Early diagenetic pyrite morphology in a mudstone-dominated succession: the Lower Jurassic Cleveland Ironstone Formation, eastern England: *Sedimentary Geology*, v. 131, p. 77–86.
- The Pandas Development Team, 2020, *pandas-dev/pandas: Pandas 1.3.0*.
- TRICHET, J., AND DÉFARGE, C., 1995, Non-biologically supported organomineralization: *Institut Oceanographique, Bulletin, Special Issue 14*, p. 203–236.
- VAN LITH, Y., WARTHMAN, R., VASCONCELOS, C., AND MCKENZIE, J.A., 2003, Microbial fossilization in carbonate sediments: a result of the bacterial surface involvement in dolomite precipitation: *Sedimentology*, v. 50, p. 237–245.
- VAREJÃO, F.G., WARREN, L.V., SIMÕES, M.G., FÜRSICH, F.T., MATOS, S.A., AND ASSINE, M.L., 2019, Exceptional preservation of soft tissues by microbial entombment: insights into the taphonomy of the Crato Konservat-Lagerstätte: *Palaios*, v. 34, p. 331–348.
- VAREJÃO, F.G., SILVA, V.R., ASSINE, M.L., WARREN, L.V., MATOS, S.A., RODRIGUES, M. G., FÜRSICH, F.T., AND SIMÕES, M.G., 2020, Marine or freshwater? Accessing the paleoenvironmental parameters of the Caldas Bed, a key marker bed in the Crato Formation (Araripe Basin, NE Brazil): *Brazilian Journal of Geology*, v. 51, e2020009.
- VAREJÃO, F.G., WARREN, L.V., SIMÕES, M.G., BUATOIS, L.A., MÁNGANO, M.G., RUMBELSPERGER, A.M.B., AND ASSINE, M.L., 2021, Mixed siliciclastic–carbonate sedimentation in an evolving epicontinental sea: Aptian record of marginal marine settings in the interior basins of north-eastern Brazil: *Sedimentology*, v. 68, p. 2125–2164.
- VASCONCELOS, C., WARTHMAN, R., MCKENZIE, J.A., VISSCHER, P.T., BITTERMANN, A.G., AND VAN LITH, Y., 2006, Lithifying microbial mats in Lagoa Vermelha, Brazil: modern Precambrian relics?: *Sedimentary Geology*, v. 185, p. 175–183.
- VILLAFANE, P.G., CONSULE-GONELLA, C., CURY, L.F., AND FARIAS, M.E., 2021, Short-term microbialite resurgence as indicator of ecological resilience against crises (Catamarca, Argentine Puna): *Environmental Microbiology Reports*, v. 13, p. 659–667.
- WARREN, L.V., VAREJÃO, F.G., QUAGLIO, F., SIMÕES, M.G., FÜRSICH, F.T., POIRÉ, D.G., CATTO, B., AND ASSINE, M.L., 2017, Stromatolites from the Aptian Crato Formation, a hypersaline lake system in the Araripe Basin, northeastern Brazil: *Facies*, v. 63, p. 1–19.
- WILKIN, R.T., BARNES, H.L., AND BRANTLEY, S.L., 1996, The size distribution of framboidal pyrite in modern sediments: an indicator of redox conditions: *Geochimica et Cosmochimica Acta*, v. 60, p. 3897–3912.
- XIONG, Y., TAN, X., WU, K., XU, Q., LIU, Y., AND QIAO, Y., 2021, Petrogenesis of the Eocene lacustrine evaporites in the western Qaidam Basin: implications for regional tectonic and climate changes: *Sedimentary Geology*, v. 416, no. 105687.
- ZEEBE, R.E., AND WOLF-GLADROW, D., 2001, *CO₂ in Seawater: Equilibrium, Kinetics, Isotopes*: Elsevier Science, Oceanography Series, v. 65, 346 p.

Received 15 October 2022; accepted 27 July 2023.